Journal of Medicinal Chemistry

Article

Structure-Activity and Structure-Conformation Relationships of Aryl Propionic Acid Inhibitors of the Kelch-like ECH-associated protein 1 : Nuclear factor erythroid 2–related factor 2 (KEAP1:NRF2) protein-protein interaction

Tom D. Heightman, James Callahan, Elisabetta Chiarparin, Joseph E. Coyle, Charlotte M. Griffiths-Jones, Ami S. Lakdawala, Rachel McMenamin, Paul Neil Mortenson, David Norton, Torren Peakman, Sharna J. Rich, Caroline Richardson, William L. Rumsey, Yolanda Sanchez, Gordon Saxty, Henriette Willems, Lawrence Wolfe, Alison J.-A. Woolford, Zining Wu, Hongxing Yan, Jeffrey K Kerns, and Thomas G. Davies

J. Med. Chem., **Just Accepted Manuscript** • DOI: 10.1021/acs.jmedchem.9b00279 • Publication Date (Web): 11 Apr 2019

Just Accepted

ACS Publications

is published by the American Chemical Society. 1155 Sixteenth Street N.W., Washington, DC 20036

Structure-Activity and Structure-Conformation Relationships of Aryl Propionic Acid Inhibitors of the Kelch-like ECH-associated protein 1 : Nuclear factor erythroid 2–related factor 2 (KEAP1:NRF2) protein-protein interaction

Tom D. Heightman[1], James F. Callahan[2], Elisabetta Chiarparin[1], Joseph E. Coyle[1], Charlotte Griffiths-Jones[1], Ami S. Lakdawala[2], Rachel McMenamin[1], Paul N. Mortenson[1], David Norton[1], Torren M. Peakman[1], Sharna J. Rich[1], Caroline Richardson[1], William L. Rumsey[2], Yolanda Sanchez[2], Gordon Saxty[1], Henriëtte M. G. Willems[1], Lawrence Wolfe III[2], Alison J.-A. Woolford[1], Zining Wu[2], Hongxing Yan[2], Jeffrey K. Kerns[2*], Thomas G. Davies[1*]

[1]Astex Pharmaceuticals, 436 Cambridge Science Park, Cambridge, CB4 0QA, UK

[2]GlaxoSmithKline, 1250 South Collegeville Road, Collegeville, PA 19426-0989, USA

*Corresponding authors

ABSTRACT

The KEAP1/NRF2-mediated cytoprotective response plays a key role in cellular homoeostasis. Insufficient NRF2 signalling during chronic oxidative stress may be associated with the pathophysiology of several diseases with an inflammatory component, and pathway activation through direct modulation of the KEAP1-NRF2 protein-protein interaction is being increasingly explored as a potential therapeutic strategy. Nevertheless, the physicochemical nature of the KEAP1-NRF2 interface suggests that achieving high affinity for a cell-penetrant drug-like inhibitor might be challenging. We recently reported the discovery of a highly potent tool compound which was used to probe the biology associated with directly disrupting the interaction of NRF2 with the KEAP1 Kelch domain. We now present a detailed account of the medicinal chemistry campaign leading to this molecule, which included exploration and optimization of protein-ligand interactions in three energetic "hot-spots" identified by fragment screening. In particular, we also discuss how consideration of ligand conformational stabilization was important to its development, and present evidence for preorganization of the lead compound which may contribute to its high affinity and cellular activity.

INTRODUCTION

The protein KEAP1 (Kelch-like ECH-associated protein 1) plays a key role in the cellular response to oxidative stress by regulating ubiquitination of the detoxification transcription factor NRF2 (Nuclear factor erythroid 2–related factor 2)[1-4]. KEAP1 consists of three domains: a N-terminal Broad-complex, Tramtrack and Bric-a-Brac (BTB) domain, which serves as an adaptor for the E3 ubiquitin ligase Cul3/Rbx1; an Intervening Region (IVR) or BACK domain; and a C-terminal Kelch repeat domain, which is a recognition module for NRF2[5-8]. Under basal conditions, NRF2 is sequestered and ubiquitinated by KEAP1/Cul3/Rbx1, before being degraded by the proteasome. Increased levels of oxidative or electrophilic stress result in covalent modification of key cysteine residues in the BTB and IVR domains, leading to dissociation of Cul3, and/or loss of productive NRF2 binding[9-12]. The KEAP1-mediated ubiquitination of NRF2 is perturbed and increasing levels of free NRF2 lead to activation of cytoprotective genes under its transcriptional control[13,14].

Inadequate NRF2-mediated signalling during chronic oxidative stress is associated with the pathophysiology of multiple diseases with an inflammatory component. As a result, KEAP1 is now well recognized as an important target for therapeutic intervention in a range of indications including respiratory, cardiovascular, renal and neurodegenerative conditions[15-21], and activation of NRF2 via covalent targeting of reactive cysteines on the BTB and IVR domains of KEAP1 is a clinically validated approach[22-25]. Recently however, direct antagonism of the Kelch-NRF2 protein-protein interaction (PPI) has been increasingly explored as an alternative point for therapeutic intervention which may offer a complementary profile[26-29]. NRF2 binds two Kelch domains in the context of dimeric KEAP1 through high affinity ("ETGE") and low affinity ("DLG") motifs which interact with a pocket at the centre of a β-propeller fold (Figure 1a), and loss of one or both of these interactions has been shown to prevent the productive engagement of NRF2 with KEAP1, with subsequent activation of the

anti-oxidant transcriptional program[30-34]. Nevertheless, the presence of multiple charged arginine residues in the NRF2-binding site associated with the tight binding of the ETGE motif, and the large and relatively solvent exposed nature of this PPI binding site suggest that achieving high affinity for a cell-penetrant drug-like molecule might be challenging[29,35].

We recently reported the application of fragment-based drug discovery (FBDD) to the Kelch domain of KEAP1, and outlined how this approach was instrumental in developing a nanomolar affinity lead, KI-696 (Figure 1a), which combined tight and selective binding to the Kelch domain with drug-like physicochemical properties, and which activates the NRF2 pathway in cell-based and animal models[36]. We now present a detailed account of the medicinal chemistry campaign leading to this lead molecule and highlight how consideration of free and bound ligand conformations were important for its development.

Figure 1

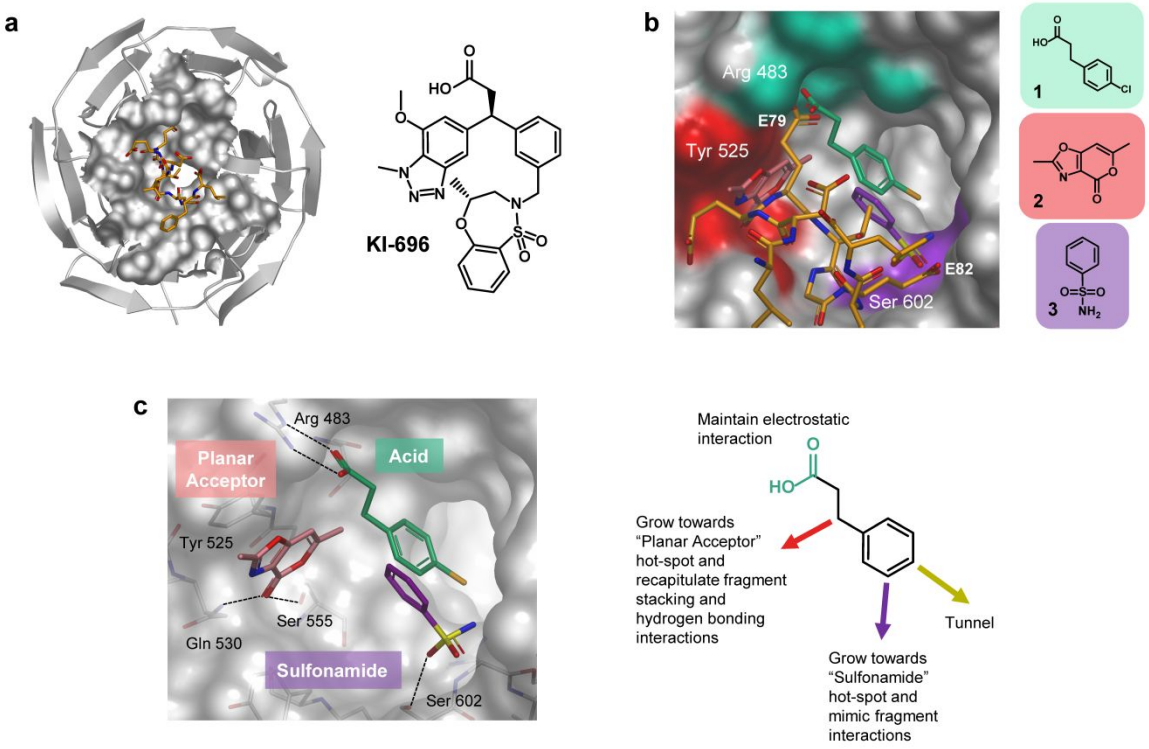

RESULTS

Insights from fragment screening and medicinal chemistry strategy

As described previously[36] fragment hits (exemplified by **1** –**3**) were observed to cluster within three main subsites or "hot-spots" in the KEAP1 Kelch-domain NRF2-binding site (Figure 1b), which we refer to here as the "Acid" ,"Planar Acceptor" and "Sulfonamide" pockets. The fragment hit 4-chlorophenylpropionic acid **1**, binding in the Acid pocket, was selected as a useful "anchor" fragment, since it provides a variety of synthetically accessible vectors for exploring the NRF2 binding site as a whole. In particular, it provides suitable vectors for accessing the other two subsites identified from the fragment screen, and the overall strategy employed was to grow from fragment **1** by introduction of functionality which could recapitulate patterns of interactions formed between fragment hits and KEAP1 in these other hot-spots (Figure 1c)[36]. Target affinity was assessed using a fluorescence polarization (FP) assay which examined the ability of compounds to displace a TAMRA-labelled NRF2-derived peptide; a subset of compounds was also selected for affinity determination by ITC. As potency was increased, compounds were additionally progressed to an MTT assay in the lung epithelial cell line BEAS-2B, which measures enzymatic activity of the NRF2-controlled oxidoreductase NQO1 (see Experimental Procedures).

SAR in the "Planar Acceptor" pocket

Inspection of the KEAP1 co-structure with hit fragment **1** (Figure 2a) suggested the benzylic position would provide a suitable vector along which to grow towards the "Planar Acceptor" pocket occupied by fragment **2**, and to introduce functionality to recapitulate the stacking and hydrogen-bonding interactions with Gln 530 and Ser 555 observed in this subsite[36]. A 3-

hydroxyphenyl group was initially introduced at this position to achieve this (compound **4**; Table 1), but did not give a measurable increase in affinity, likely due to the mismatch of the hydroxyl presenting both hydrogen bond acceptor and donor functionality where a double acceptor motif would be preferred as observed with fragment **2**. In contrast, replacement of this ring system with the hydroxy pyridine **5** gave the first analogue with measurable potency in the fluorescence polarization assay, suggesting that this compound binds as the pyridone tautomer. The co-crystal structure of **5** with the Kelch domain confirmed the anticipated binding mode, in which the pyridine ring stacks with Tyr 525, and the pyridone carbonyl accepts hydrogen bonds from Gln 530 and Ser 555 (Figure 2b) as observed for fragment hit **2**. Subsequent methylation of the nitrogen to fix the pyridone tautomer provided compound **6** with an FP IC_{50} value of 260 μM.

We hypothesised that interactions in the Planar Acceptor pocket might be enhanced by replacing the pyridone with a fused bicyclic heterocycle, such that adjacent heteroatoms would accept the two hydrogen-bonds from Gln 530 and Ser 555, as well as increasing π-stacking with Tyr 525. This approach afforded a 4-5-fold enhancement in potency in the methyl benzotriazole **7**, which formed the expected pattern of stacking and polar interactions (Figure 2c)[36]. The methyl benzotriazole proved the most potent among the isosteric heterocycles tested: the pyridotriazole **8** and benzisoxazole **9** both showed approximately 5-fold weaker binding compared with **7**, possibly due to differences in hydrogen bond acceptor strength or π-stacking complementarity with Tyr 525. Other heterocycles without the ability to undergo the double acceptor interaction, such as the indazole **10** or imidazopyridine **11**, also showed weaker binding.

Table 1 Structure activity relationships for 3-substituted 4-chlorophenylpropionic acids. FP IC_{50} displacement of NRF2 peptide from KEAP1 Kelch protein by fluorescence polarization assay. K_d for direct binding to KEAP1 Kelch protein by ITC.

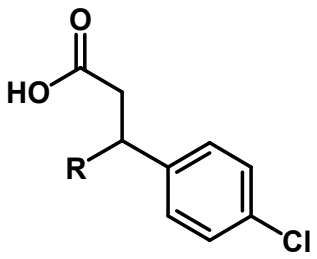

Compound	R	FP IC_{50}/μM[a]	ITC K_d/μM[b]
1[†]	H	>1000 (*n*=2)	-
4	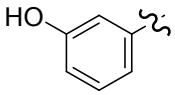	>1000 (*n*=1)	-
5	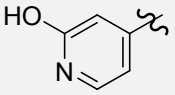	40% @ 300 (*n*=2)	-
6	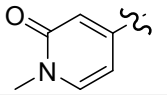	260 (*n*=2)	-
7[†]	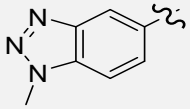	61 (*n*=4)	59
(*R*)-**7**	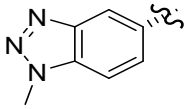	170 (*n*=2)	-
(*S*)-**7**	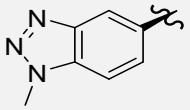	47 (*n*=3)	-
8	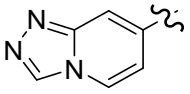	330 (*n*=1)	-
9	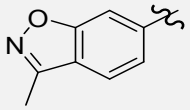	66% @ 300 (*n*=2)	-
10	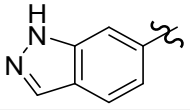	57% @ 300 (*n*=1)	-
11	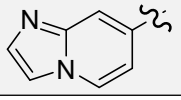	47% @ 300 (*n*=1)	-

[a]Geometric mean of independent determinations. [b]Single determination. Note that ITC data were measured for the racemate. [†]Data for compounds **1** and **7** is taken from Davies et al[36].

Figure 2

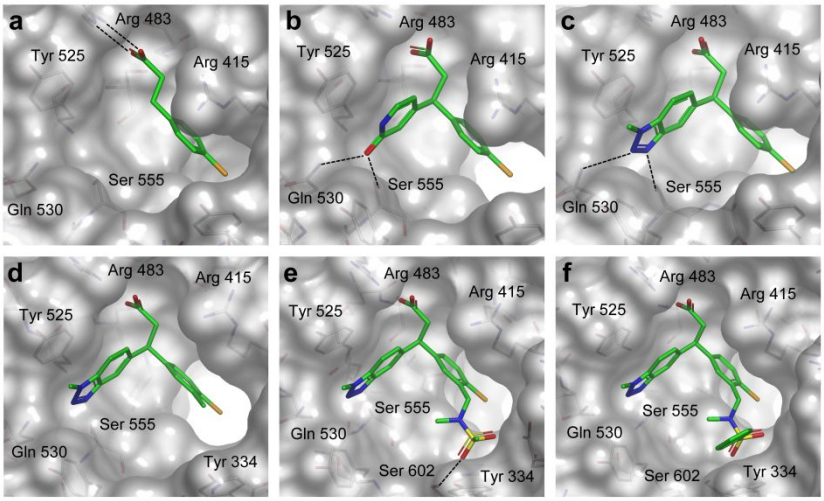

SAR in the "Sulfonamide" pocket

Having established the methyl benzotriazole as an efficient binder in the Planar Acceptor pocket, we next sought to exploit the "Sulfonamide" binding pocket identified by fragment **3** (Figure 1c), through growth *ortho* to the chloro substituent[36]. Extension of **7** in this manner with either a methyl (**12**) or hydroxymethyl (**13**) group did not afford additional potency (Table 2); however, the co-structure of **12** confirmed the desired orientation for the growth vector, with the methyl pointing towards the Sulfonamide pocket rather than into the tunnel region at the centre of the Kelch domain (Figure 2d). This suggested that attachment of a sulfonamide *via* nitrogen to a methylene carbon should allow the sulfonamide oxygens to occupy similar positions to those in the structure of fragment **3**. Indeed, the *N*-methyl methanesulfonamide **14** achieved a potency enhancement of approximately 18-fold compared with **7**, and as described previously[36], the co-crystal structure of **14** confirmed the intended binding mode, in which one sulfonamide oxygen accepts a hydrogen bond from the side chain of Ser 602 (Figure 2e). This structure also highlighted an opportunity for further potency gain, as the sulfonyl methyl group

is oriented towards the aromatic ring of Tyr 334 and the lipophilic edge of the binding site. Replacement of this methyl group with a phenyl (**15**) gave a further 13-fold affinity enhancement, taking the IC_{50} value to 270 nM[36]. As previously reported, the co-structure of the benzenesulfonamide analogue **15** confirmed a similar binding mode to that of **14**, while its additional phenyl ring is well aligned to engage in π-stacking and lipophilic interactions with Tyr 334 (Figure 2f)[36]. SAR to explore alternative aromatic substituents in this region was relatively flat, with replacement by electron poor (pyridine **16**) and electron rich (dimethylpyrazole **17**) heterocycles having only small effects on affinity. Replacement with a saturated ring system (cyclohexyl **18**) reduced affinity, potentially indicating the importance of π-stacking and shape complementarity in addition to lipophilicity for optimal interaction in this area of the site.

Only the (*S*)-enantiomers of compounds prepared as racemates were observed to bind by X-ray crystallography, but separation of the enantiomers of **7** showed only a modest eudysmic ratio (Table 1), and a co-structure of the single (*R*)-enantiomer of **7** with KEAP1 could also be obtained, indicating that the methylene linker possesses enough flexibility to allow key pharmacophore points to be reached without a major energetic penalty. Interestingly, X-ray crystallographic analysis of Kelch soaked with (*R*)-**7** also revealed clear electron density for a second ligand binding event adjacent to the canonical pose, interacting with the lipophillic edge of the NRF2 site and co-binding with a molecule of DMSO from the soaking solution (Figure 3). For our previously published KEAP1 co-structures with bis-aryl compounds, we had observed residual electron density at this position which we speculated to arise due to the binding of a second ligand molecule at the high concentrations employed during the soaking experiments[36]. In these cases however, the low occupancy and high levels of disorder (as evident from weak and broken electron density) precluded the fitting of these additional sites with confidence. As discussed later, the chloro-phenyl moiety for the second copy of (*R*)-**7,**

and the co-bound molecule of DMSO may highlight additional, albeit weaker hot-spots for favourable interaction which were not evident from the main fragment screen.

Figure 3

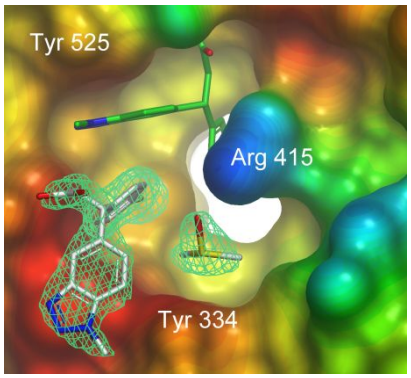

Inspection of the co-structure of **15** suggested that the ligand might be bound in an energetically unfavourable conformation, due to the relatively close approach of the chloro substituent and one of the sulfonamide oxygens ($r_{Cl...O}$ = 3.7 Å) (Figure 4a). We hypothesised that replacement of the chloro-substituent with a methyl group might relieve this unfavourable intramolecular contact, as this change would replace the negative electrostatic potential at the edge of the chloro with a positive electrostatic potential arising from the C-H bond polarization in the methyl group (Figure 4b). A 3-dimensional conformational search on a reduced model system (Figure 4c), suggested that with the chloro substituent, the bound conformation is approximately 2 kcal mol^{-1} higher in energy than the gas-phase global minimum. By contrast, the global energy minimum for the methyl analogue is the same as (or very close to) the bound conformation (see Supporting Information). Although the full potential energetic benefit of this change was not realized, presumably due to additional competing factors, this optimization nevertheless led to a small increase in target affinity (compound **19**). In addition, this

compound also gave the first measurable activity in a cell-based assay, with stimulation of NQO1 activity in the human lung epithelial cell line, BEAS-2B (Table 2). A methoxy group was subsequently introduced at the benzotriazole 7-position with the aim of increasing the hydrogen bonding potential of the ring nitrogens through electron donation, and to add additional surface contacts[36], and this afforded an additional small increase in target affinity and cellular potency (compound **20**).

Table 2 Structure activity relationships for substituted phenyl methylbenzotriazole propionic acids. FP IC_{50} displacement of NRF2 peptide from KEAP1 Kelch protein by fluorescence polarization assay; K_d for direct binding to KEAP1 Kelch protein by ITC; BEAS-2B EC_{50} in NQO1 MTT assay.

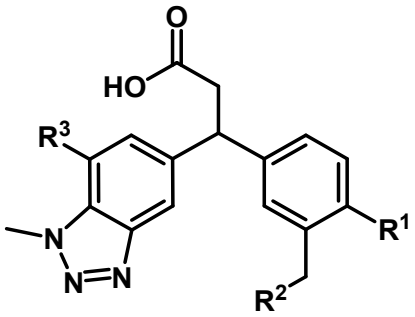

Compound	R^1	R^2	R^3	FP IC_{50}/μM[a]	ITC K_d/μM[b]	BEAS-2B EC_{50}/μM[c]
12	Cl	H	H	44 (*n*=2)	-	-
13	Cl	OH	H	140 (*n*=2)	-	-
14[†]	Cl	$NMeSO_2Me$	H	3.4 (*n*=3)	4.0	-
15[†]	Cl	$NMeSO_2Ph$	H	0.27 (*n*=3)	0.67	-
16	Cl	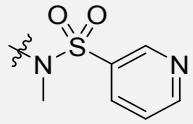	H	0.58 (*n*=2)	-	-
17	Cl	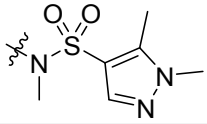	H	0.32 (*n*=1)	-	-
18	Cl	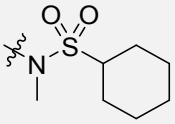	H	2.4 (*n*=16)	-	-
19	Me	$NMeSO_2Ph$	H	0.13 (*n*=3)	0.11	3.4 (*n*=8)
20	Me	$NMeSO_2Ph$	OMe	0.069 (*n*=10)	0.044	0.85 (*n*=13)
21	Me	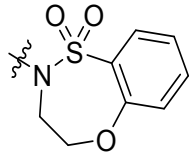	OMe	0.047 (*n*=12)	0.035	1.6 (*n*=14)
22	Me	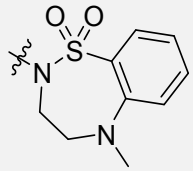	OMe	0.037 (*n*=12)	-	0.57 (*n*=14)

23	Me	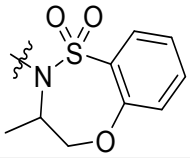	OMe	0.26 (*n*=10)	-	1.4 (*n*=14)
24	Me	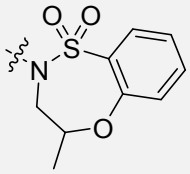	OMe	0.020 (*n*=10)	-	0.030 (*n*=14)
25	H	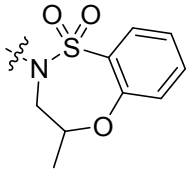	OMe	0.18 (*n*=6)	-	2.9 (*n*=6)

[a]Geometric mean of independent determinations. [b]Single determinations. Note that ITC data for all compounds were measured for racemates. [c]Geometric mean of independent determinations. [†]Data for compounds **14** and **15** is taken from Davies et al[36].

Figure 4

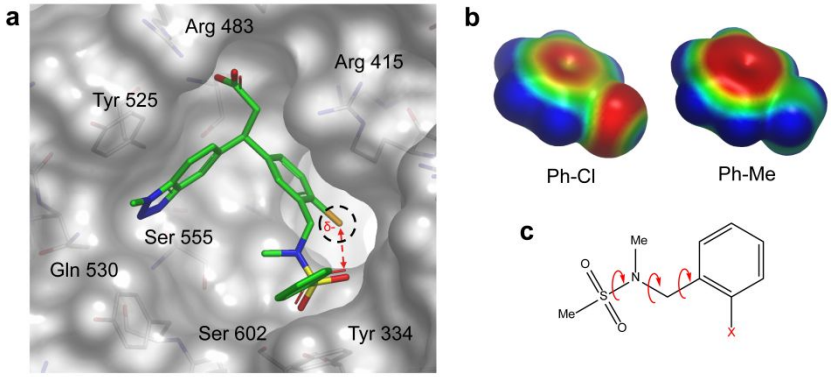

As the sulfonamide **20** appeared to interact with most of the polar and π-stacking features in the NRF2-binding pocket (Figure 5a), we considered approaches other than optimizing non-covalent interactions to further enhance the affinity and cellular potency. Ligand conformational rigidification can be a favourable strategy to achieve enhanced binding affinity and this approach has been used recently for other PPI inhibitors[37]. The co-structure of KEAP1-

20 suggested geometric and steric suitability for cyclization of the phenyl sulfonamide to form the fused 7-membered benzoxathiazepine **21**, potentially pre-organizing this lower part of the molecule in the bound conformation to give increased affinity. The co-structure of **21** with Kelch confirmed the expected binding mode (Figure 5b), with only minor perturbation to the canonical interactions; however, cyclization led to a void between the oxathiazepine and benzotriazole in the bound conformation of **21** (Figure 5c), which may be energetically unfavourable. To address this, we therefore explored the introduction of small lipophilic substituents (eg methyl) to both oxathiazepine and thiadiazepine rings, which modelling suggested would partially fill this unoccupied space (compounds **22-24**).

Figure 5

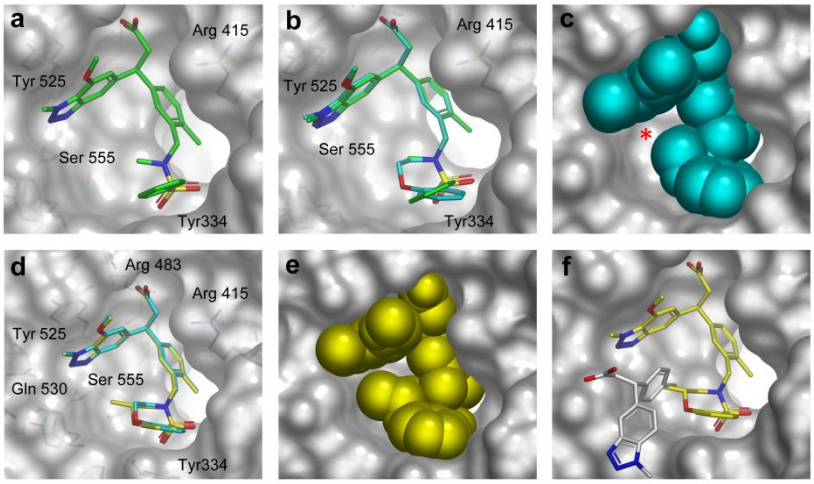

Substitution at the position alpha to the oxathiazepine oxygen was predicted to be optimal for space-filling, and addition of methyl at this location gave the largest increase in affinity (**24**). Subsequent KEAP1 co-soaks with **24**, which contained a mixture of four diastereomers, revealed preferential binding of the (*R,S*) isomer. A subsequent study of the separate

stereoisomers of **24** (Table 3) confirmed (*R,S*) as the highest affinity configuration (**29** (KI-696); K_d 1.3 nM; BEAS-2B EC_{50} 12 nM)[36], consistent with minimal perturbation from the binding mode of **21**, and occupation of the space between oxathiazepine and benzotriazole by the "pendant" pseudo-equatorial methyl (Figure 5d-e). Interestingly this methyl also occupies the pocket region where the chloro-phenyl binds for the second copy of (*R*)-**7**, highlighting the energetic benefits of space-filling and lipophilic interactions in this part of the binding site (Figure 5f).

Table 3 Structure-activity relationships for stereoisomers of **24**. FP IC_{50} displacement of NRF2 peptide from KEAP1 Kelch protein by fluorescence polarization assay; K_d for direct binding to KEAP1 Kelch protein by ITC; BEAS-2B EC_{50} in NQO1 MTT assay.

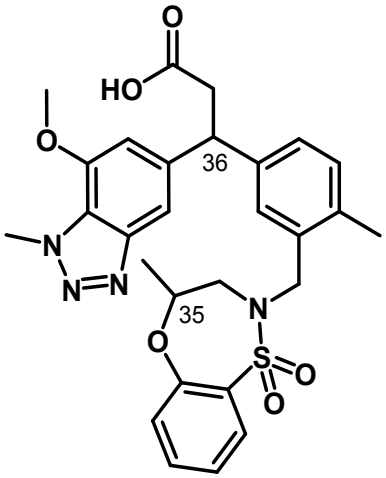

Compound	Configuration @35	Configuration @36	FP IC_{50}/μM[a]	ITC K_d/μM[b]	BEAS-2B EC_{50}/μM[c]
26	*R*	*R/S*	0.010 (*n*=12)	-	0.011 (*n*=12)
27	*S*	*R/S*	0.042 (*n*=10)	-	0.76 (*n*=12)
28	*R*	*R*	0.024 (*n*=18)	-	0.083 (*n*=20)
29[†]	*R*	*S*	95%@15nM (*n*=3)	0.0013	0.012

[a]Geometric mean of independent determinations. [b]Single determination. [c]Geometric mean of independent determinations. [†]Data for compound **29** is taken from Davies et al[36].

NMR solution conformational studies for free ligands

In addition to relieving the possible energetic penalty associated with the void observed for the KEAP1-bound **21**, we hypothesised that introduction of the pendant C35 methyl (Figure 6a) might favour a preorganized conformation of the free ligand through a "hydrophobic collapse" between the benzotriazole heterocycle, the central phenyl and the oxathiazepine as observed in the bound state; it could also lead to local conformational restriction of the seven-membered ring due to the preference to maintain the methyl group in an pseudo-equatorial position. Both modes of preorganization might be expected to lead to an increase in affinity over more conformationally flexible analogues on entropic grounds. In addition, we speculated that the large increase in cellular potency observed for **29** compared to **21** might in part arise due to increased cell permeability which could result from reduced molecular flexibility[38].

To examine the validity of this hypothesis experimentally, ^{1}H 1D and 2D ^{1}H-^{1}H ROESY spectra were acquired in aqueous solution for **20**, **21** and **29**. An initial observation from the ^{1}H 1D spectra was that the diastereotopic protons on the phenyl-sulfonamide methylene linker (19′ and 19″, Figure 6) gave widely separated chemical shifts for **29**, with a $\Delta\delta$ of 0.59 ppm, potentially indicating restricted rotation around C19-C29 and/or C19-N37 bonds. This contrasts with the singlet resonances observed for the methylene protons for des-Me **21**, and uncyclized **20** (Figure 6b), typical of averaging of the electronic environment due to ligand flexibility.

Figure 6

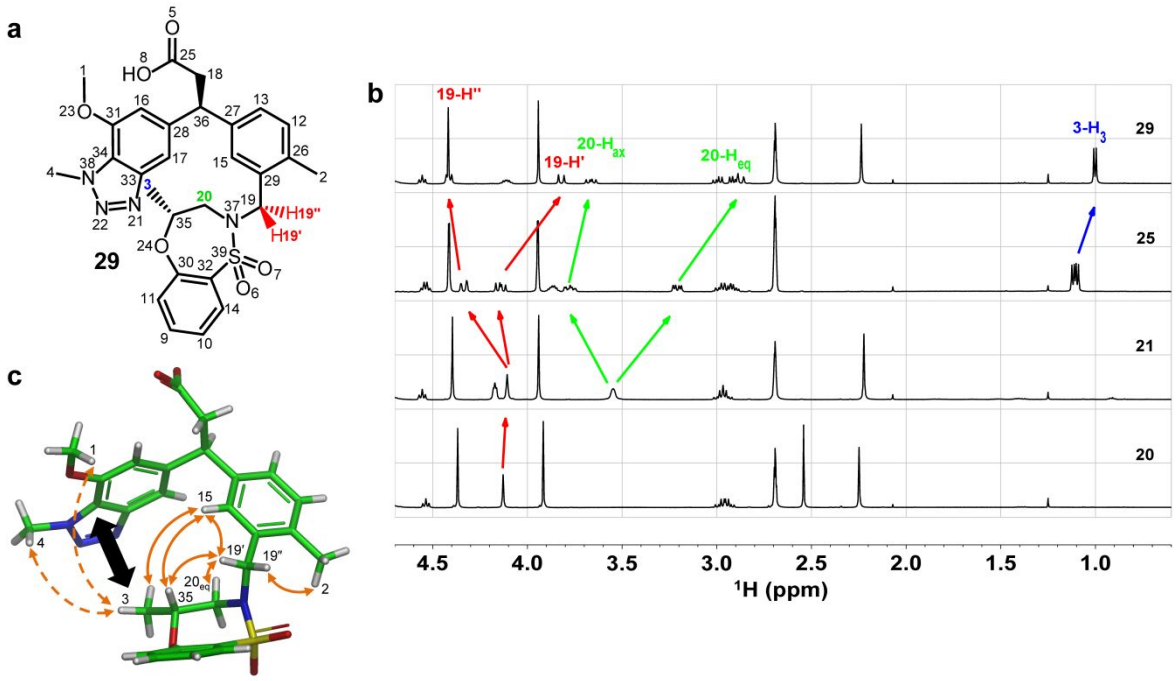

To preclude the possibility that the large Δδ between 19′ and 19″ for **29** might be due to chemical inequivalence, a ^{1}H 1D spectrum was also acquired for the simpler analogue **25**, which retains the oxathiazepine methyl stereocentre, but was anticipated to be more conformationally flexible due to the loss of the tolyl methyl. For this compound, a smaller Δδ (0.19 and 0.21 ppm for the diastereoisomers) was observed between the methylene protons (Figure 6b), suggesting that the larger Δδ observed between 19′ and 19″ in **29** is not solely a result of their diastereotopic character. Further evidence for a preferred conformation for the methylene linker in **29** was supported by the pattern of ROEs to/from 19′ and 19″, which are consistent with the placement of 19′ and 19″ in different environments as observed in the bound pose with KEAP1 (Figure 6c and Supporting Information Figure 1a). The pattern of ROEs between the benzoxathiazepine ring and the central phenyl ring (specifically with proton 15) is also consistent with **29** adopting a conformation in which the relative orientation of these parts

of the molecule is close to that observed when bound to KEAP1 (Figure 6c and Supporting Information Table 1).

For the des-Me analogues (**21** and **25**), a weakening of the analogous ROEs (Supporting Information Table 1) suggests a greater conformational flexibility for this part of the molecule, with a greater range of conformations adopted in solution compared to **29**. Finally, for **29**, distinct axial (3.66, dd, *J*=15.0, 10.4 Hz) and equatorial (2.87, d, *J*=15.0 Hz) signals were observed for 20-H_2 in the seven-membered ring, consistent with a single pseudo-chair conformation with the pendant methyl pseudo-equatorial as observed for the bound structure. In contrast, for the des-Me **21**, averaged signals were observed for the protons on the seven-membered ring, suggesting a high degree of conformation mobility and rapid exchange between axial and equatorial positions (Figure 6b).

For **29**, weak ROEs between the pendant methyl and the benzotriazole methyl and the methoxy were also observed, consistent with a "collapsed" conformation similar to that observed bound to KEAP1 (Figure 6c and Supporting Information Figure 1b). Further evidence for this comes from a small shielding (0.1 ppm) of the pendant methyl (3-H_3) in **29** compared to **25** (Figure 6b), in agreement with a population of a collapsed conformation with the pendant methyl over the face of the benzotriazole. In addition, shielding (0.34 ppm) of **29** 20-H_{eq} compared to **25** is observed (Figure 6b), in agreement with this hydrogen lying over the central phenyl ring as observed in the conformation bound to KEAP1.

Taken together, these observations are consistent with the hypothesis that introduction of the pendant methyl leads to increased preorganization for **29**, potentially through a combination of local conformation restriction, and hydrophobic collapse. In contrast, both the des-Me analogue **21**, and the uncyclized **20** exhibit features suggesting a greater degree of mobility and a lack of preferred conformation, consistent with their lower affinity. The comparison with **25**, which is

also considerably less potent in both FP and BEAS-2B assays compared to **29** (Tables 2 and 3), suggests that the presence of the tolyl methyl group on the central phenyl ring is also a key structural element in reducing the number of conformations around the methylene group, and in increasing the population of the bioactive conformation.

Synthesis

The 3-hydroxyphenyl analogue **4** was synthesized according to Scheme 1. Addition of the Grignard reagent **30** to 4-chlorobenzonitrile followed by hydrolytic workup afforded the benzophenone **31**. Next, a Wittig reaction using trimethyl phosphonoacetate followed by nickel borohydride reduction of the resulting unsaturated ester gave the bisarylpropionate ester **32**, which was demethylated using boron tribromide to give the acid **4**.

The preparation of hydroxypyridine **5** and methylpyridone **6** mirrored the procedure for **4**, as shown in Scheme 2. Addition of 4-chlorophenylmagnesium bromide to the cyanomethoxy pyridine **33** followed by a Wittig reaction and nickel borohydride reduction gave the methoxypyridyl ester **34**. This was either doubly demethylated using 4M HCl to give **5**, or rearranged to the *N*-methylpyridone with methyl iodide followed by basic ester hydrolysis to give **6**.

Synthesis of the *N*-methyl benzotriazole **7** in racemic form was described previously[36]. The enantiomers were separated using chiral HPLC to provide (*R)*-**7** and (*S*)-**7**.

The triazolopyridine analogue **8** was prepared according to Scheme 3. The triazolopyridyl carboxylic acid **35** was converted to the Weinreb amide **36** by HBTU coupling, and treatment with 4-chlorophenyl magnesium bromide gave the ketone **37**. A similar sequence to Schemes 1-2 involving a Wittig reaction, conjugate reduction and ester hydrolysis gave **8**.

The benzisoxazole **9** was prepared by a more concise route outlined in Scheme 4. Oxidative cyclisation of ketone **39** with ammonia followed by NCS gave the bromo benzisoxazole **40**[39] which was converted to the boronate ester **41** under standard conditions. Next, a rhodium catalysed conjugate addition[40] to methyl 4-chlorocinnamate followed by saponification gave the bisaryl propionic acid analogue **9** directly. The indazole **10** and imidazopyridine **11** were prepared similarly from the corresponding boronate esters.

The 4-chloro-3-methyl analogue **12** was prepared according to Scheme 5. Here, the benzotriazolyl aldehyde **42** was converted to the cinnamate **43** by a Wittig reaction, upon which rhodium catalysed conjugate addition of the pinacol boronate ester, followed by saponification gave **12**.

The synthesis of compounds **13-15** was described previously[36]. The pyridyl sulfonamide **16** was prepared by conversion of the sulfonyl chloride **44** to the methylsulfonamide **45**, which was then subjected to a Mitsunobu alkylation with the hydroxymethyl compound **46**[36], followed by saponification to give **16** (Scheme 6). Sulfonamides **17** and **18** were prepared by a similar sequence starting from their corresponding sulfonyl chlorides.

Compound **19** containing a methyl group in place of the Cl in the preceding compounds was prepared by a complementary route outlined in Scheme 7. First the cinnamate **43**[36],was coupled with 3-hydroxymethyl-4-methyl phenyl boronic acid using rhodium catalysis to give intermediate **51**, and then a Mitsunobu coupling with *N*-methyl benzenesulfonamide followed by saponification gave **19**. The methoxy-substituted triazole analogue **20** was prepared *via* an analogous sequence starting from the corresponding methoxybenzotriazolyl acrylate ester[36].

Syntheses of the fused 7-membered ring analogues **21**-**24** are outlined in Scheme 8. Compound **21** was prepared by a Mitsunobu coupling of commercial benzoxathiazepine **52** with the hydroxymethyl intermediate **53**[36], followed by saponification of the ester. Compound **22** was prepared similarly: reaction of 2-fluorobenzenesulfonamide with 2-(methylamino)ethanol

followed by cyclization under Mitsunobu conditions gave the benzthiadiazepine **56**, which was again coupled with **53** under Mitsunobu conditions followed by saponification. The isomeric methylated benzoxathiazepine analogues **23** and **24** were prepared by reaction of 2-fluorobenzenesulfonyl chloride (**58**) with 2-amino-1-propanol or 1-amino-2-propanol respectively, followed by cyclization under microwave conditions to give **60** and **63** respectively, which were then coupled with **53** and saponified as above.

The desmethyl analogue **25** was prepared according to Scheme 9, by coupling the methoxybenzotriazolyl acrylate ester under rhodium catalysis to 3-hydroxymethylphenyl boronic acid, followed by Mitsunobu coupling with the methylated benzoxathiazepine **63** and subsequent saponification.

The stereoisomers **26**-**29** were prepared by analogy to compound **24**, following the route outlined in Scheme 8 and using the appropriate enantiomer of 1-amino-2-propanol to set the configuration at C35, followed by chiral SFC separation to isolate single diastereoisomers at C36.

Scheme 1

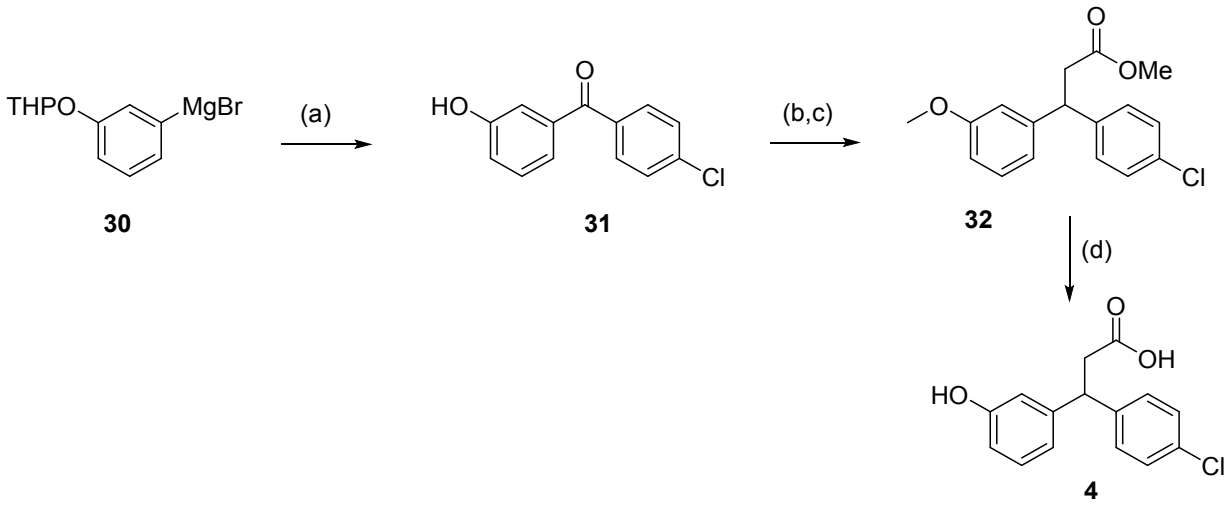

a) 4-Cl-PhCN, THF, 75 °C, then HCl (aq), 45%. b) Trimethyl phosphonoacetate, KO^{t}Bu, THF, 0 °C, 69%. c) $NiCl_2.6H_2O$, $NaBH_4$, MeOH, 0 °C, 88%. d) BBr_3, DCM, -42 °C to RT, 34%.

Scheme 2

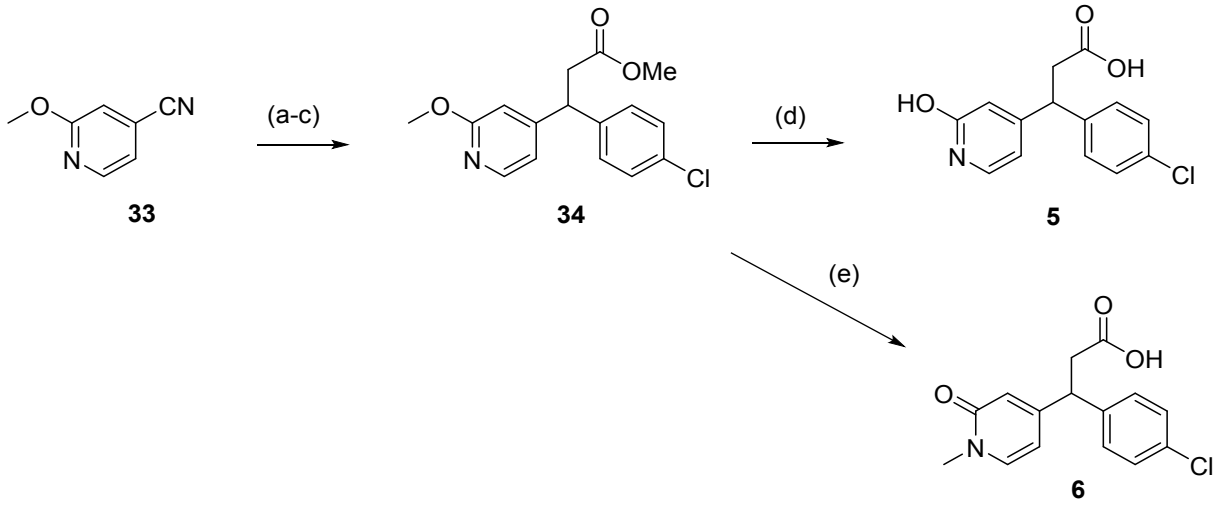

a) 4-Cl-PhMgBr, THF, 75 °C. b) Trimethyl phosphonoacetate, KO^{t}Bu, THF, 0 °C. c) $NiCl_2.6H_2O$, $NaBH_4$, MeOH, 0 °C, 69% over 3 steps. d) 4M HCl, 1,4-dioxane, 60 °C, 34%. e) Neat MeI, 100 °C, workup then 2M NaOH, MeOH, 50%.

Scheme 3

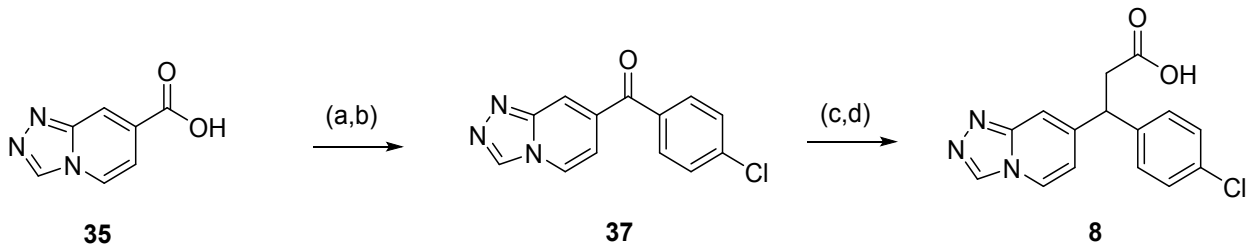

a) MeONHMe, HBTU, *N*-methylmorpholine, DCM, DMF, 47%. b) 4-Cl-PhMgBr, THF, 0 °C, 64%. c) Trimethyl phosphonoacetate, KO^{t}Bu, THF, 0 °C, 44%. d) $NiCl_2.6H_2O$, $NaBH_4$, MeOH, 0 °C, then NaOH, MeOH, 9% over two steps.

Scheme 4

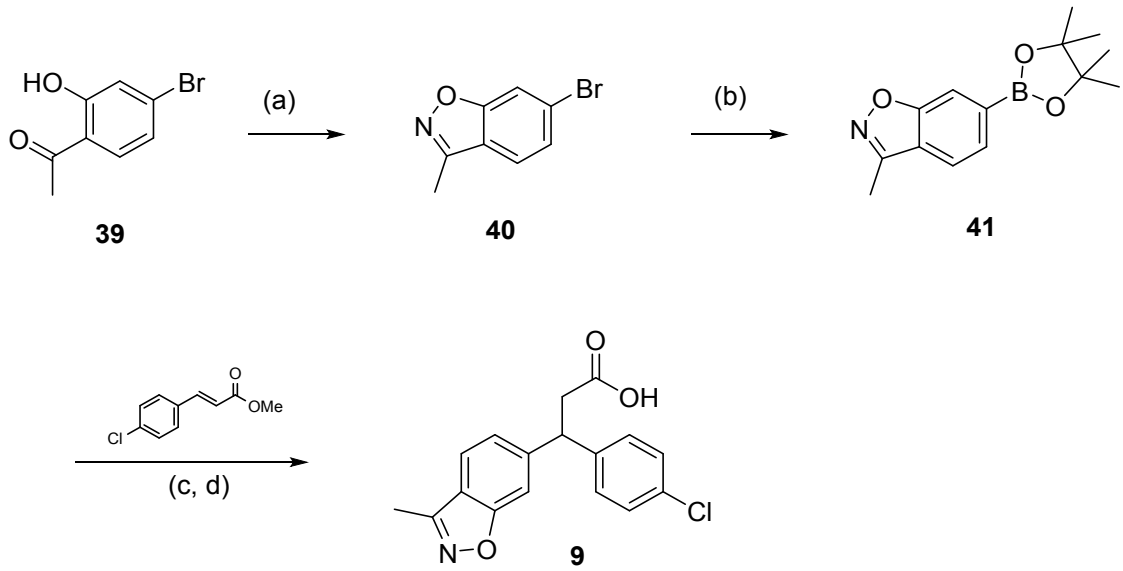

a) NH_3, MeOH, then NCS, K_2CO_3, THF, 21%. b) $(Bpin)_2$, KOAc, 1,4-dioxane, $PdCl_2dppf$, 90 °C, 76%. c) $[RhCl(cod)]_2$, 1,4-dioxane/water, Et_3N, 95 °C, 67%. d) 1M LiOH, MeOH, 7%.

Scheme 5

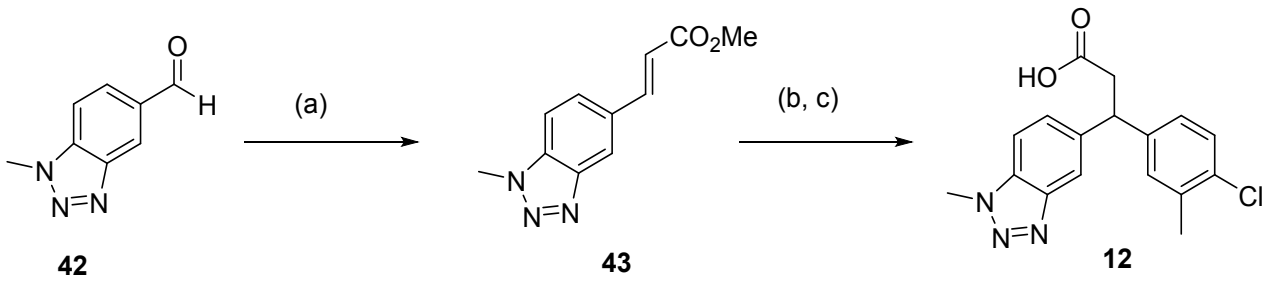

a) Trimethyl phosphonoacetate, KO^{t}Bu, THF, 0 °C, quant. b) [RhCl(cod)]$_2$, 1,4-dioxane/water, Et$_3$N, 95 °C. c) 1M LiOH, MeOH, 41% over 2 steps.

Scheme 6

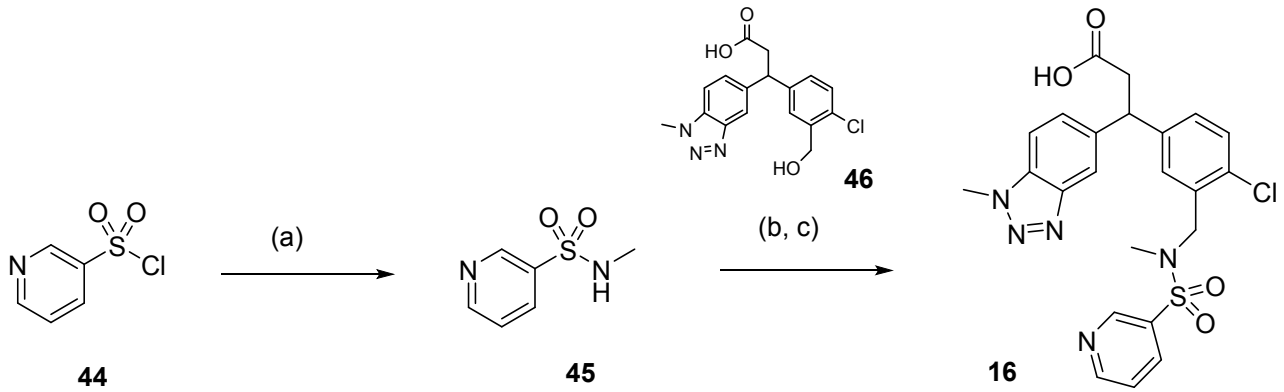

a) MeNH$_2$, DCM/THF, 98%. b) ADDP, ^{t}Bu$_3$P, THF. c) 1M LiOH, MeOH,13% over 2 steps.

Scheme 7

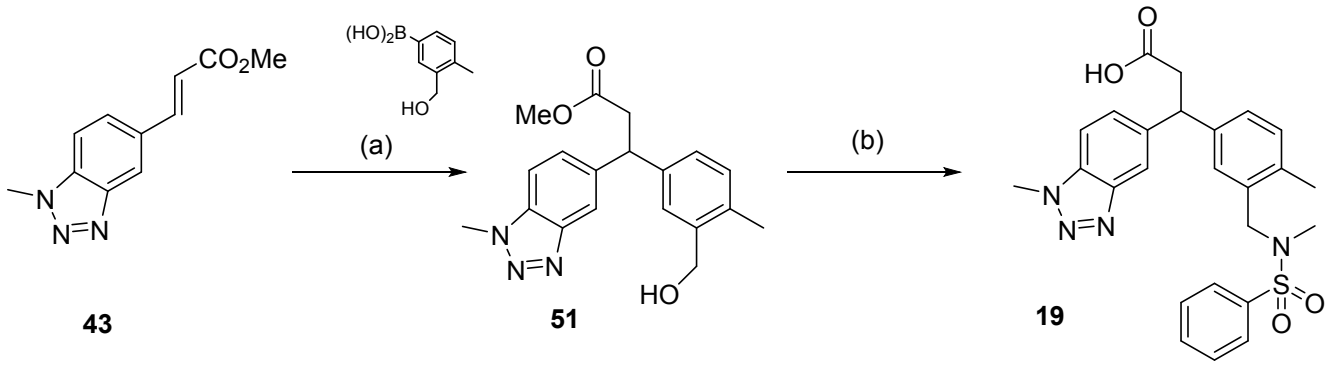

a) [RhCl(cod)]$_2$, 1,4-dioxane/water, Et$_3$N, 95 °C, 45%. b) PhSO$_2$NHMe, ADDP, ^{n}Bu$_3$P, THF, then 3M NaOH (aq), 30%.

Scheme 8

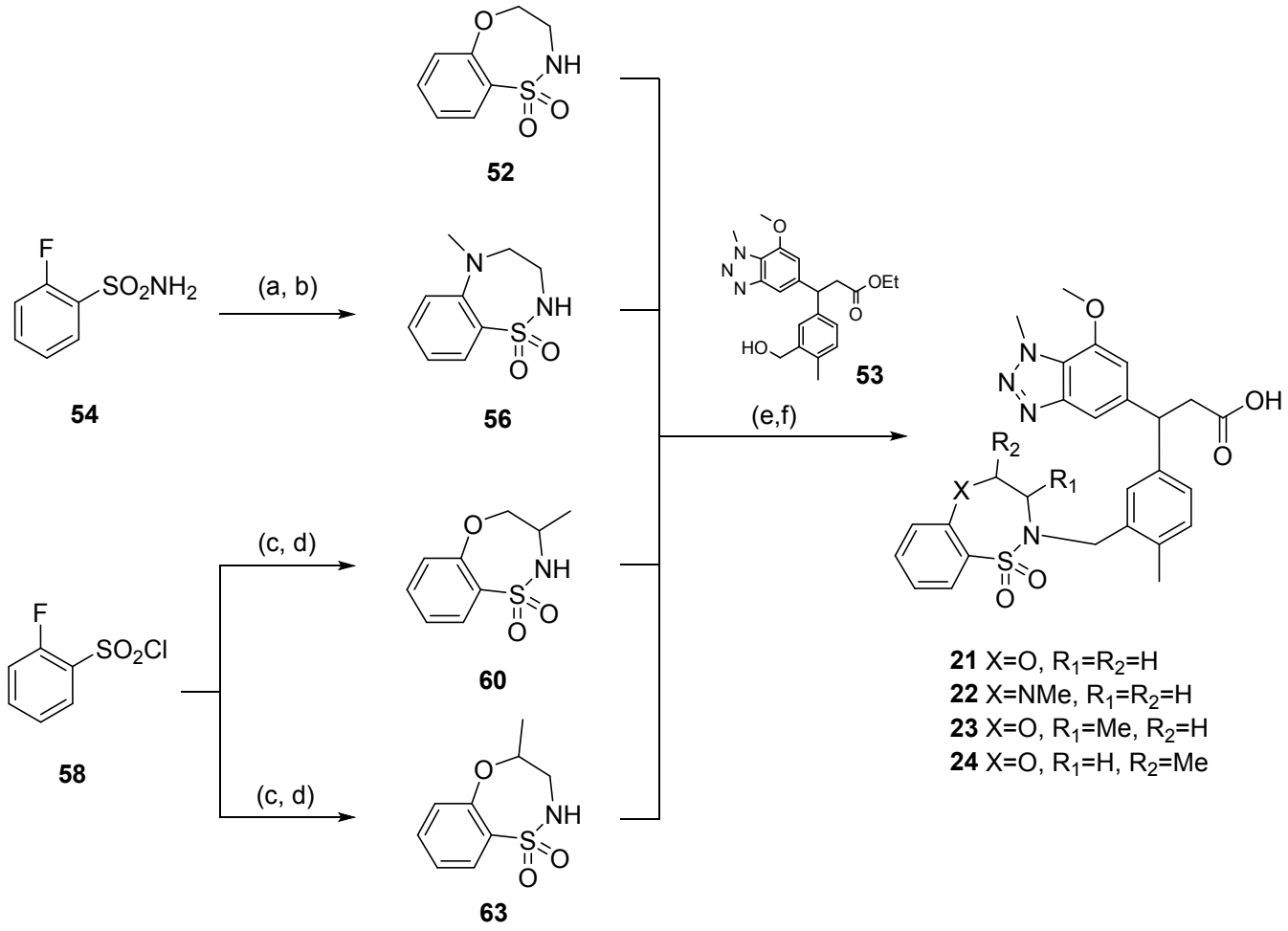

a) $MeNHCH_2CH_2OH$, 130 °C microwave, 87%. b) DIAD, PS-PPh_3, THF, 73%. (c) 2-Amino-1-propanol or 1-amino-2-propanol, K_2CO_3, THF, quant. (d) KO^tBu, DMSO, microwave cyclization, quant. (**60**); 88% (**63**). e) ADDP, Bu_3P or DIAD, PS-PPh_3, THF. f) NaOH (aq. 2M), MeOH.

Scheme 9

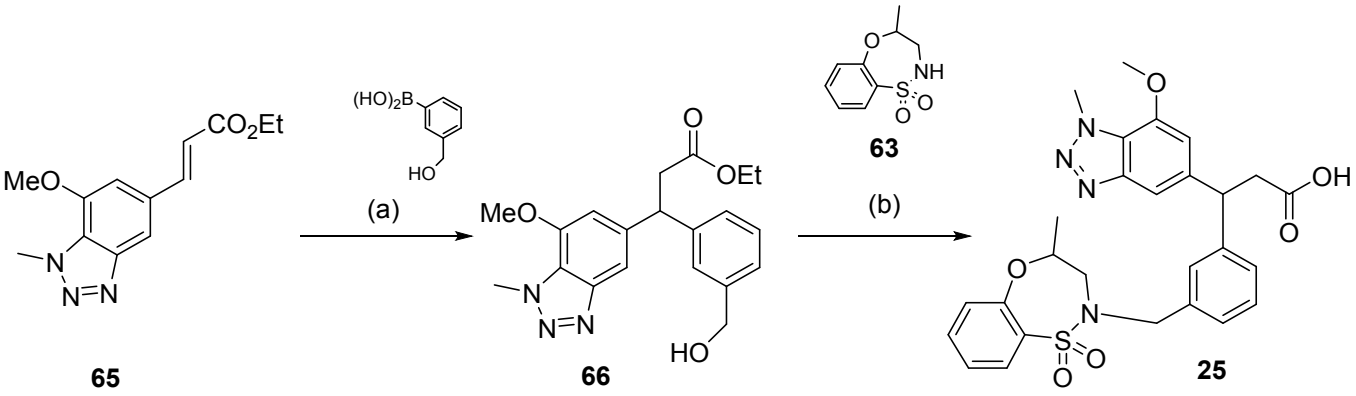

a) $[RhCl(cod)]_2$, 1,4-dioxane/water, Et_3N, 150 °C, 55 %. b) DIAD, PS-PPh_3, THF, then 1M NaOH (aq.), MeOH, 100 °C, 38 %.

DISCUSSION AND CONCLUSIONS

We have described here a detailed account of the medicinal chemistry campaign which led to the identification of KI-696 (**29**), a highly potent inhibitor of the KEAP1 Kelch-NRF2 interaction, and activator of the NRF2 pathway in cell-based assays, primary cells and *in vivo*[21,36]. As outlined previously, fragment screening identified three distinct "hot-spots" within the NRF2 binding pocket of KEAP1, providing information which was used to progress a weak fragment hit (K_d >1 mM) to molecules with nanomolar affinity for KEAP1[36]. Of particular importance was evidence that non-charged moieties can bind close to the region occupied by the NRF2 Glu 82 side-chain, and this insight assisted in the development of a highly potent lead containing only a single acidic functionality, allowing good cell permeability to be achieved[36].

The structure-driven elaboration from millimolar fragment to nanomolar lead described in this study highlights two important approaches to structure-guided affinity improvement. The first is exploiting the insight into favourable intermolecular interactions afforded by fragment screening. The prediction of protein-ligand energetics *ab initio* remains challenging and identifying and targeting specific polar interactions to provide gains in affinity can be particularly difficult due to competition with solvent binding. Recapitulating patterns of protein-ligand interactions known empirically to improve affinity is a useful strategy for addressing this limitation; for example, through exploitation of SAR and binding modes from previous hit matter, or through virtual screening driven by interaction fingerprints[41-44]. Fragment screening is in theory well suited to give such information, but in practice, it is unusual to observe a collection of hits that provide an energetic mapping of the whole binding site of interest. Exploitation of weaker interactions throughout a target's binding pocket ("warm-spots") can also be an important means to build potency[45], but such sites may not always be readily detectable using standard fragment screening protocols. In this study

however, three discrete subsites were identified through X-ray fragment screening, providing direct insight into multiple molecular recognition points, and allowing a rapid and efficient improvement in affinity. Further insight into favourable interaction sites was also provided by observation of an additional lower occupancy ligand binding event at high soak concentrations, as well as the co-binding of DMSO, which could be considered to represent an additional, "ultra-low" molecular weight fragment.

A second important route to increasing affinity is through designs which seek to stabilize energetically unfavourable aspects of the bound ligand pose, and/or to pre-organize the ligand in the bound conformation. This approach is particularly beneficial in the context of inhibiting protein-protein interactions, because it may allow affinity gains to be achieved without addition of molecular weight and/or polar surface area. This has been exemplified recently by a series of IAP PPI inhibitors in which a folded conformation was stabilized in solution by an apparent attractive interaction of complementary partial charges between a nitrogen lone pair and a carbonyl carbon[37].

In this study, we believe the driving force for the folded conformation of **29** arises from the hydrophobic effect, rather than explicitly attractive contacts (such as van der Waals dispersion or CH-π interactions) for two reasons. Firstly, systematic studies using Wilcox balance systems have shown that van der Waals forces between hydrocarbon motifs are weak, such that solvent-solvent interactions have a dominant role in driving the association of apolar groups[46]. Secondly, the distance between the methyl and centroid of the triazole ring system of Kelch-bound **29** is rather long at approximately 4 Å, compared to CSD mean distances for similar methyl CH-π interactions (3.5 Å),[47] although we note that this distance may be influenced by the interaction of **29** with the protein, with a slightly closer approach of methyl and benzotriazole possible in the unbound state. Interestingly, a potentially analogous methyl-π

contact was observed in a series of orexin receptor antagonists in which NMR suggested the preferential presence of a U-shaped conformer in solution, placing a methyl group in proximity to the π-system of a benzofuran ring[48]. In this case, a subsequent X-ray structure of a related ligand bound to the orexin-1 receptor showed a shorter methyl-π system distance of 3.5 Å[49], which might be indicative of a genuine CH-π interaction.

Finally, although NRF2 is an intrinsically disordered protein, with no stable tertiary structure, there is evidence that the local region of polypeptide forming the ETGE β-turn may also be partially pre-organized in solution[32,50,51]. However, the mechanism by which the natural ligand and compound **29** achieve this preorganization is very different: in the case of NRF2 through extensive intramolecular hydrogen bonding within the secondary structure of the turn motif, and for **29** through the hydrophobic collapse described above. For **29** the preorganization is achieved far more efficiently, with the result that a much higher proportion of its molecular weight comprises functionality which forms direct interactions with the pocket[36]. Taken together, the insight into molecular recognition provided by fragment screening, the structure-driven optimization of hot-spot interactions, and the experimental and theoretical consideration of free ligand conformation, have all provided important contributions to the development of a potent lead molecule with good physicochemical properties, and promising biological activity in cellular and animal disease models.

EXPERIMENTAL PROCEDURES

*Synthesis of compounds **4-66***

All solvents and commercially available reagents were used as received. All reactions were followed by TLC analysis (TLC plates GF254, Merck) or LC-MS (liquid chromatography mass spectrometry). LC-MS analysis was performed with an Agilent or Shimadzu LC system with variable wavelength UV detection using reverse phase chromatography with a CH_3CN and water gradient with a 0.02 or 0.1% TFA modifier (added to each solvent) and using a reverse phase column, e.g., Thermo Hypersil Gold C18. MS was determined using either PE Sciex 150EX LC-MS, Waters ZQ LC-MS, or Agilent 6140 LC-MS Single Quadrupole instruments. Column chromatography was performed on prepacked silica gel columns (3090 mesh, IST) using a Biotage SP4 or similar. NMR spectra are referenced as follows: ^{1}H (400 MHz), internal standard TMS at $\delta = 0.00$. Abbreviations for multiplicities observed in NMR spectra: s; singlet; br s, broad singlet; d, doublet; t, triplet; q, quadruplet; p, pentuplet; spt, septuplet; m, multiplet. All compounds reported are of at least 95% purity according to LC-MS unless stated otherwise.

3-(4-Chlorophenyl)-3-(3-hydroxyphenyl)propanoic acid (4)

A solution of methyl 3-(4-chlorophenyl)-3-(3-methoxyphenyl)propanoate **32** (122 mg, 0.40 mmol) in DCM (2 mL) under N_2 was treated with BBr_3 (0.116 mL 1.21 mmol) dropwise at -42 °C. The mixture was slowly allowed to warm to room temperature overnight. The reaction was then quenched by slowly adding water. After stirring for another 30 minutes the product was extracted with $CHCl_3$:IPA (3:1, x3). The combined organic layers were washed with brine and dried over $MgSO_4$. The product was filtered and concentrated in vacuo, and the residue purified by preparative HPLC to yield 3-(4-chlorophenyl)-3-(3-hydroxyphenyl)propanoic acid **4** (38 mg, 34%) as a colourless solid. ^{1}H NMR (DMSO-d_6): 7.33-7.26 (m, 4H), 7.04 (t, $J = 7.8$,

1H), 6.70 (d, *J* = 7.6, 1H), 6.64-6.62 (m, 1H), 6.55 (dd, *J* = 8.0, 2.4, 1H), 4.33 (t, *J* = 7.8, 1H), 2.81 (d, *J* = 7.7, 2H). LCMS (Acidic_RR02): *m/z* 294 $[M+18]^+$, RT = 1.26 min. Purity >95%.

3-(4-Chlorophenyl)-3-(2-hydroxypyridin-4-yl)propanoic acid (5).

A solution of 4-chlorophenylmagnesium bromide in THF (1M, 2.3 mL, 2.33 mmol) was added to neat 4-cyano-2-methoxypyridine **33** (260 mg, 1.94 mmol) under N_2. The reaction mixture was refluxed for 2 hours at 75 °C, and then allowed to cool. The solution was then poured into carefully into HCl (1M, aq.). The product was extracted with DCM (x3) and the combined organic layers were washed with water, and brine before being dried with anhydrous $MgSO_4$. The filtrate was concentrated to dryness in vacuo to yield 4-(4-chlorobenzoyl)-2-methoxypyridine as an orange oil (~0.6 g, >85% pure) which was used without further purification. LCMS (Acidic_RR02): *m/z* 248 $[M+H]^+$, RT = 1.46 min. A solution of ^{t}BuOK (327 mg, 2.91 mmol) in THF (19 mL) at 0 °C was treated with trimethyl phosphonoacetate (705 µL, 4.27 mmol), under N_2. After 10 mins, the 4-(4-chlorobenzoyl)-2-methoxypyridine was added slowly. The reaction was stirred for 2 hours, while being allowed to warm to room temperature and then quenched with NH_4Cl (aq., sat.). The mixture was diluted with water and then extracted with *n*-heptane (x3). The combined organic layers were washed with water and brine and dried over $MgSO_4$. The product was filtered and evaporated in vacuo to yield methyl 3-(4-chlorophenyl)-3-(2-methoxypyridin-4-yl)prop-2-enoate as a pale yellow solid (0.5 g, ~90% pure). LCMS (Acidic_RR02): *m/z* 304 $[M+H]^+$, RT = 1.51 min. To methyl 3-(4-chlorophenyl)-3-(2-methoxypyridin-4-yl)prop-2-enoate under N_2 was added the MeOH and then $NiCl_2.6H_2O$ (90 mg, 0.38 mmol). The reaction was cooled to 0 °C, and then sodium borohydride was added slowly in portions. The mixture became black and effervescence noted. After the reaction mixture was stirred for 16 h at room temperature, the reaction was quenched with NH_4Cl (sat., aq.) and diluted with EtOAc. The organic layer was separated and dried over

$MgSO_4$, filtrated and concentrated under reduced pressure to yield methyl 3-(4-chlorophenyl)-3-(2-methoxypyridin-4-yl)propanoate **34** (410 mg, 69%). ^{1}H NMR (Me-d_3-OD): 8.02 (d, J = 5.5 Hz, 1H), 7.34-7.29 (m, 4H), 6.87 (d, J = 5.6 Hz, 1H), 6.78-6.74 (m, 1H), 4.50 (t, J = 7.6 Hz, 1H), 3.89 (s, 3H), 3.60 (s, 3H), 3.15-3.08 (m, 2H). LCMS (Acidic_RR02): *m/z* 306 $[M+H]^+$, RT = 1.4 min. >75% pure.

Methyl 3-(4-chlorophenyl)-3-(2-methoxypyridin-4-yl)propanoate **34** (90 mg, 0.29 mmol) and 4M HCl aq (0.70 mL) in 1,4-dioxane (1.5 mL) was heated at 60 °C for 4 hours in a reacti vial. The reaction was then diluted with water and the product extracted with $CHCl_3$:IPA (3:1, x2). The combined organic layers were washed with water, brine and dried over $MgSO_4$. The product was filtered, evaporated in vacuo, and purified by preparative HPLC to yield 3-(4-chlorophenyl)-3-(2-hydroxypyridin-4-yl)propanoic acid **5** as a pale yellow solid (28 mg, 34%). ^{1}H NMR (Me-d_3-OD): 7.39-7.27 (m, 5H), 6.51 (s, 1H), 6.34 (dd, J = 6.8, 1.8, 1H), 4.39 (t, J = 7.8, 1H), 3.12-2.96 (m, 2H). LCMS (Acidic_RR02): *m/z* 278 $[M+H]^+$, RT = 1.06 min. Purity >95%.

3-(4-Chlorophenyl)-3-(1-methyl-2-oxo-1,2-dihydropyridin-4-yl)propanoic acid (6).

Methyl 3-(4-chlorophenyl)-3-(2-methoxypyridin-4-yl)propanoate **34** (70 mg, 0.17 mmol, 75% pure) and MeI (500 mg) were heated to 100 °C for 4 hours in a reacti vial. The reaction was allowed to cool and was then evaporated in vacuo. LCMS (Acidic_RR02): *m/z* 306 $[M+H]^+$, RT = 1.22 min. The residue was taken up in MeOH (3 mL) and 2M NaOH (3 mL, aq.), and stirred for 30 minutes at room temperature. The reaction was diluted with water and acidified with 5% citric acid (aq.). The product was extracted with $CHCl_3$:IPA (3:1, x3). The combined organic layers were washed with brine and dried over $MgSO_4$. The product was filtered, evaporated in vacuo and purified by preparative HPLC to yield 3-(4-chlorophenyl)-3-(1-methyl-2-oxo-1,2-dihydropyridin-4-yl)propanoic acid **6** (25 mg, 50%) as colourless oil. ^{1}H

NMR (Me-d_3-OD): 7.53 (d, J = 7.0, 1H), 7.35-7.27 (m, 4H), 6.51 (d, J = 1.9, 1H), 6.29 (dd, J = 7.0, 2.0, 1H), 4.36 (t, J = 7.9, 1H), 3.52 (s, 3H), 3.06 (dd, J = 16.1, 8.0, 1H), 2.99 (dd, J = 16.1, 7.7, 1H). LCMS (Acidic_RR02): *m/z* 292 $[M+H]^+$, RT = 1.11 min. Purity >95%.

(*R*) and (*S*) 3-(4-Chlorophenyl)-3-(1-methyl-1*H*-1,2,3-benzotriazol-5-yl)propanoic acid ((*R*)-7) and (*S*)-7).

A sample of rac-3-(4-chlorophenyl)-3-(1-methyl-1*H*-1,2,3-benzotriazol-5-yl)propanoic acid **7** was subjected to chiral chromatography (Phenomenex Lux Cellulose-2 column (250x4.6mm for analytical, 250x21.2mm for purification), mobile phase 70:30 heptane:ethanol +0.1% TFA) to give the two individual enantiomers:

(3*R*)-3-(4-chlorophenyl)-3-(1-methyl-1*H*-1,2,3-benzotriazol-5-yl)propanoic acid (*R*)-**7**) (39 mg, 49%) as a colourless solid. ^{1}H NMR (Me-d_3-OD): 7.93-7.90 (m, 1H), 7.68 (dd, J = 8.8, 1.0, 1H), 7.49 (dd, J = 8.7, 1.6, 1H), 7.36-7.28 (m, 4H), 4.73 (t, J = 7.9, 1H), 4.31 (s, 3H), 3.26-3.08 (m, 2H). LCMS (Acidic_RR02): *m/z* 316 $[M+H]^+$, RT = 1.25 min. Purity >95%.

(3*S*)-3-(4-chlorophenyl)-3-(1-methyl-1*H*-1,2,3-benzotriazol-5-yl)propanoic acid (*S*)-**7**) (34 mg, 43%) as a colourless solid. ^{1}H NMR (Me-d_3-OD): 7.93-7.91 (m, 1H), 7.68 (d, J = 8.7, 1H), 7.49 (dd, J = 8.7, 1.6, 1H), 7.36-7.28 (m, 4H), 4.73 (t, J = 8.0, 1H), 4.31 (s, 3H), 3.26-3.08 (m, 2H). LCMS (Acidic_RR02): *m/z* 316 $[M+H]^+$, RT = 1.25 min. Purity >95%.

3-(4-Chlorophenyl)-3-{[1,2,4]triazolo[4,3-a]pyridin-7-yl}propanoic acid (8)

To methyl 3-(4-chlorophenyl)-3-{[1,2,4]triazolo[4,3-a]pyridin-7-yl}prop-2-enoate **38** (90 mg, 0.22 mmol) was added MeOH (5.0 mL) under nitrogen and then $NiCl_2.6H_2O$ (11 mg, 0.04 mmol). The reaction was cooled to 0 °C and sodium borohydride (25 mg, 0.67 mmol) was added slowly in portions. The mixture became black and effervescence noted. After stirring for 4 hours at room temperature, the reaction was quenched with NH_4Cl (sat., aq.). The product

was extracted with EtOAc. The organic layer was separated and dried over $MgSO_4$, filtrated and concentrated under reduced pressure. To the residue was added NaOH (1M, 2 mL) and MeOH (4 mL) and the mixture was stirred at room temperature for 30 minutes. The reaction was diluted and the pH adjusted to ~pH 4-5 with 2M HCl. The product was extracted with $CHCl_3$:IPA (3:1, x2). The combined organic layers were washed with water, brine and dried over $MgSO_4$. The product was filtered, evaporated in vacuo and purified by preparative HPLC to yield 3-(4-chlorophenyl)-3-{[1,2,4]triazolo[4,3-a]pyridin-7-yl}propanoic acid **8** as colourless solid (8 mg, 9%). ^{1}H NMR (Me-d_3-OD): 9.10 (d, J = 1.0, 1H), 8.38 (dd, J = 7.1, 1.1, 1H), 7.39-7.32 (m, 5H), 6.92 (dd, J = 7.2, 1.6, 1H), 4.63 (t, J = 7.9, 1H), 3.21 (dd, J = 16.1, 8.1, 1H), 3.12 (dd, J = 16.1, 7.7, 1H). LCMS (Acidic_RR02): *m/z* 302 $[M+H]^+$, RT = 1.11 min. Purity >95%.

3-(4-Chlorophenyl)-3-(3-methyl-1,2-benzoxazol-6-yl)propanoic acid (9)

A solution of 3-methyl-6-(4,4,5,5-tetramethyl-1,3,2-dioxaborolan-2-yl)-1,2-benzoxazole **41** (202 mg), methyl (2*E*)-3-(4-chlorophenyl)prop-2-enoate (77 mg) and triethylamine (0.08 mL) in 1,4-dioxane (4 mL) and water (0.4 mL) was degassed by bubbling through nitrogen for 10 minutes. $[RhCl(cod)]_2$ (10 mg) was added and the mixture was heated to 95 °C overnight. The reaction was cooled and the mixture partitioned between water (20 mL) and ethyl acetate (3 x 20 mL). The combined organic fractions were dried over $MgSO_4$, filtered and concentrated. The residue was columned in 0-50% ethyl acetate and petrol to give methyl 3-(4-chlorophenyl)-3-(3-methyl-1,2-benzoxazol-6-yl)propanoate (173 mg, 69%). LCMS $[M+H]^+$ 330. A mixture of methyl 3-(4-chlorophenyl)-3-(3-methyl-1,2-benzoxazol-6-yl)propanoate (173 mg), methanol (1 mL) and 1M lithium hydroxide solution (3 mL) was stirred 4 hours at room temperature. 1M lithium hydroxide solution (1 mL) was added and the reaction stirred overnight at room temperature. Potassium hydroxide (300 mg) was added and the mixture was

stirred for 4 hours at room temperature and 4 hours at 60 °C. The pH was adjusted to pH 5 with 1M HCl and the product was extracted with IPA:$CHCl_3$ (1:3 v/v) (3 x 20 mL). The combined organic fractions were washed with brine, dried over $MgSO_4$, filtered and concentrated to give the desired product **9** (12 mg, 7%). ^{1}H NMR (Me-d_3-OD): 7.65 (1H, d), 7.54 (1H, s), 7.34-7.25 (5H, m), 4.73 (1H, t), 2.96 (2H, dd), 2.57-2.52 (3H, m). LCMS $[M+H]^+$ 316.

3-(4-Chlorophenyl)-3-(1*H*-indazol-6-yl)propanoic acid (10)

Methyl 4-chlorocinnamate (150 mg, 0.76 mmol), 6-indazolyboronic acid (140 mg, 0.86 mmol), $[RhCl(cod)]_2$ (19 mg, 0.04 mmol) and triethylamine (159 µL, 1.14 mmol) in 1,4-dioxane (2.5 mL) and water (0.4 mL) was heated in a reacti vial at 95 °C for 18 hours. The reaction was allowed to cool and then NaOH (1M, 2 mL) was added. The reaction stirred at room temperature for 4 hours, after which it was diluted with water and the pH was adjusted to ~pH 4-5 with HCl (aq, 1M). The product was extracted with $CHCl_3$:IPA (3:1, x3). The combined organic layers were washed with brine and dried over $MgSO_4$. The product was filtered, evaporated in vacuo, and purified by preparative HPLC to yield 3-(4-chlorophenyl)-3-(1*H*-indazol-6-yl)propanoic acid **10** as yellow solid (3 mg, 1%). ^{1}H NMR (Me-d_3-OD): 7.98 (d, J = 1.1, 1H), 7.68 (d, J = 8.5, 1H), 7.46 (s, 1H), 7.34-7.27 (m, 4H), 7.06 (dd, J = 8.4, 1.4, 1H), 4.67 (t, J = 7.9, 1H), 3.11 (dd, J = 7.9, 2.3, 2H). LCMS (Basic_RR01): *m/z* 301 $[M+H]^+$, RT = 0.99 min. Purity >90%.

3-(4-Chlorophenyl)-3-{imidazo[1,2-a]pyridin-7-yl}propanoic acid (11)

Methyl 4-chlorocinnamate (150 mg, 0.76 mmol), 7-(4,4,5,5-tetramethyl-[1,3,2]dioxaborolan-2-yl)-imidazo[1,2-a]pyridine (200 mg, 0.82 mmol), $[RhCl(cod)]_2$ (19 mg, 0.04 mmol) and triethylamine (159 µL, 1.14 mmol) in 1,4-dioxane (2.5 mL) and water (0.4 mL) was heated in a reacti vial at 95 °C for 18 hours. The reaction was allowed to cool and then NaOH (1M, 2

mL) was added. The reaction stirred at room temperature for 4 hours, after which it was diluted with water and the pH was adjusted to ~pH 4-5 with HCl (aq, 1M). The product was extracted with $CHCl_3$:IPA (3:1, x3). The combined organic layers were washed with brine and dried over $MgSO_4$. The product was filtered, evaporated in vacuo, and purified by preparative HPLC to yield 3-(4-chlorophenyl)-3-{imidazo[1,2-a]pyridin-7-yl}propanoic acid **11** as a colourless solid (3 mg, 1%). >90% pure. 0.5 FA salt. ^{1}H NMR (Me-d_3-OD): 8.43 (d, J = 7.1, 1H), 7.87 (d, J = 5.4, 1H), 7.66 (d, J = 2.0, 1H), 7.58 (s, 1H), 7.38-7.31 (m, 4H), 6.98 (dd, J = 7.0, 1.8, 1H), 4.64 (t, J = 7.8, 1H), 3.17 (dd, J = 15.7, 7.8, 1H), 3.10 (dd, J = 15.9, 7.8, 1H). LCMS (Basic_RR01): *m/z* 301 $[M+H]^+$, RT = 0.99 min. Purity >95%.

3-(4-Chloro-3-methylphenyl)-3-(1-methyl-1*H*-1,2,3-benzotriazol-5-yl)propanoic acid (12)

1-Methyl-1*H*-1,2,3-benzotriazole-5-carbaldehyde (2.0 g, 12.4 mmol) and methyl (triphenylphosphoranylidene)acetate (5.9 g, 3.7 mmol) in toluene (31 mL) was heated at 95 °C for 2 hours and then allowed to cool. The product was filtered to yield methyl (2*E*)-3-(1-methyl-1*H*-1,2,3-benzotriazol-5-yl)prop-2-enoate **43** as a pale peach solid (3.1 g, 114%). LCMS (Acidic_RR02): *m/z* 218 $[M+H]^+$, RT = 1.18 min. Purity 90%. Methyl (2*E*)-3-(1-methyl-1*H*-1,2,3-benzotriazol-5-yl)prop-2-enoate **43** (100 mg, 0.41 mmol, 90% pure), 4-chloro-3-methylphenylboronic acid (141 mg, 0.83 mmol), $[RhCl(cod)]_2$ (10 mg, 0.02 mmol) and triethylamine (0.86 µL. 0.62 mmol) in 1,4-dioxane (1.4 mL) and water (0.2 mL) was heated in a reacti vial to 95 °C for 18 hours. The reaction was allowed to cool to room temperature and NaOH (1M, 2 mL) was added. The mixture was stirred for 4 hours and then diluted with water. The pH was adjusted to ~pH 4 with HCl (aq, 1M) and the product extracted with $CHCl_3$:IPA (3:1, x3). The combined organic layers were washed with brine and dried over $MgSO_4$. The product was filtered, evaporated in vacuo and purified by preparative HPLC to yield 3-(4-chloro-3-methylphenyl)-3-(1-methyl-1*H*-1,2,3-benzotriazol-5-yl)propanoic acid **12** as a

colourless oil (56 mg, 41%). ^{1}H NMR (Me-d_3-OD): 7.90 (s, 1H), 7.62 (d, J = 8.6, 1H), 7.45 (dd, J = 8.6, 1.6, 1H), 7.28-7.23 (m, 2H), 7.15-7.10 (m, 1H), 4.67 (t, J = 7.9, 1H), 4.28 (s, 3H), 3.21-3.08 (m, 2H), 2.31 (s, 3H). LCMS (Basic_RR01): *m/z* 330 $[M+H]^+$, RT = 0.99 min. Purity >95%.

3-{4-Chloro-3-[(N-methylpyridine-3-sulfonamido)methyl]phenyl}-3-(1-methyl-1H-1,2,3-benzotriazol-5-yl)propanoic acid (16)

1,1'-Azodicarbonyldipiperidine (168 mg) and tri-*tert*-butyl phosphine (109 µl) were added to a solution of *N*-methylpyridine-3-sulfonamide **45** (57 mg) and methyl 3-(4-chloro-3-(hydroxymethyl)phenyl)-3-(1-methyl-1*H*-benzo[d][1,2,3]triazol-5-yl)propanoate **46** (120 mg). The resulting mixture was stirred at room temperature overnight. More 1,1'-azodicarbonyldipiperidine (84 mg) and tri-*tert*-butyl phosphine (55 µl) were added and the reaction was stirred 4 hours more. Lithium hydroxide (3 mL of a 1M solution) was added and the mixture was stirred for 3 hours. The reaction mixture was partitioned between water and ethyl acetate. The aqueous fraction was adjusted to pH 5 with 1M HCl and extracted with IPA:$CHCl_3$ (1:3 v/v) (3x 20 mL). The combined organic fractions were dried over $MgSO_4$, filtered and concentrated and the residue purified by preparative HPLC to give 3-{4-chloro-3-[(*N*-methylpyridine-3-sulfonamido)methyl]phenyl}-3-(1-methyl-1H-1,2,3-benzotriazol-5-yl)propanoic acid **16** (22 mg). ^{1}H NMR (Me-d_3-OD): 8.98 (1H, d), 8.88-8.76 (1H, m), 8.30-8.18 (1H, m), 7.89 (1H, s), 7.76-7.60 (2H, m), 7.60-7.44 (1H, m), 7.41 (1H, s), 7.36-7.25 (2H, m), 4.75 (1H, t), 4.53-4.34 (2H, m), 4.34-4.25 (3H, m), 3.07-2.88 (2H, m), 2.82-2.64 (3H, m). LCMS $[M+H]^+$ 500.

3-{4-Chloro-3-[(N-methyl1,5-dimethyl-1H-pyrazole-4-sulfonamido)methyl]phenyl}-3-(1-methyl-1H-1,2,3-benzotriazol-5-yl)propanoic acid (17)

1,1'-Azodicarbonyldipiperidine (177 mg) and tri-*tert*-butyl phosphine (180 µl) were added to a solution of *N*,1,5-trimethyl-1*H*-pyrazole-4-sulfonamide **47** (66 mg) and methyl 3-[4-chloro-3-(hydroxymethyl)phenyl]-3-(1-methyl-1*H*-1,2,3-benzotriazol-5-yl)propanoate (125 mg) in THF (Davies *et al*[36], compound 20). The resulting mixture was stirred at room temperature overnight. More 1,1'-azodicarbonyldipiperidine (177 mg) and tri-*tert*-butyl phosphine (180 µl) were added and the reaction was stirred 48 hours more. The reaction mixture was partitioned between water (10 mL) and ethyl acetate (2 x 10 mL). The combined organic fractions were dried over $MgSO_4$, filtered and concentrated. The residue was columned in 0-10% methanol and DCM to give methyl 3-{4-chloro-3-[(*N*-methyl-1,5-dimethyl-1*H*-pyrazole-4-sulfonamido)methyl]phenyl}-3-(1-methyl-*1H*-1,2,3-benzotriazol-5-yl)propanoate (400 mg). Purity 60%. ^{1}H NMR (Me-d_3-OD): 8.04 (1H, s), 8.00-7.89 (1H, m), 7.76 (1H, s), 7.75-7.68 (1H, m), 7.47 (1H, s), 7.44-7.25 (2H, m), 4.53-4.43 (3H, m), 4.27 (2H, s), 3.88 (3H, s), 3.77-3.55 (3H, m), 3.37 (3H, s), 3.26 (1H, dd), 2.76-2.59 (3H, m), 2.54 (2H, s). LCMS $[M+H]^+$ 531. A mixture of methyl 3-{4-chloro-3-[(*N*-methyl1,5-dimethyl-1*H*-pyrazole-4-sulfonamido)methyl]phenyl}-3-(1-methyl-1H-1,2,3-benzotriazol-5-yl)propanoate (200 mg), 1M lithium hydroxide (2 mL) and methanol (2 mL) was stirred for 2 h at room temperature. DCM (10 mL) and water (10 mL) were added and the layers were separated. The aqueous fraction was adjusted to pH 4 with 1M HCl and extracted with IPA:$CHCl_3$ (1:3 v/v) (3x 20 mL). The combined organic fractions were dried over $MgSO_4$, filtered and concentrated and the residue purified by preparative HPLC to give 3-{4-chloro-3-[(*N*-methyl1,5-dimethyl-1*H*-pyrazole-4-sulfonamido)methyl]phenyl}-3-(1-methyl-1*H*-1,2,3-benzotriazol-5-yl)propanoic acid **17** (9 mg, 5%). ^{1}H NMR (Me-d_3-OD): 7.93-7.85 (1H, m), 7.73 (1H, s), 7.66 (1H, d), 7.50

(1H, d), 7.45-7.36 (1H, m), 7.36-7.25 (2H, m), 4.79-4.70 (1H, m), 4.31 (3H, s), 4.25 (2H, s), 3.86 (3H, s), 3.00 (2H, d), 2.58 (3H, s), 2.52 (3H, s). LCMS $[M+H]^+$ 517.

3-(4-Chloro-3-((*N*-methylcyclohexanesulfonamido)methyl)phenyl)-3-(1-methyl-1*H*-benzo[d][1,2,3]triazol-5-yl)propanoic acid (18)

To a solution of methyl 3-(4-chloro-3-((*N*-methylcyclohexanesulfonamido)methyl)phenyl)-3-(1-methyl-1*H*-benzo[d][1,2,3]triazol-5-yl)propanoate **50** (82 mg, 0.15 mmol) in MeOH (4 mL) stirred at ambient temperature was added a solution of 1M LiOH (10 mL, 10.00 mmol). The solution became a suspension and then diluted with MeOH (6 mL). The reaction mixture was stirred at ambient temperature for 1 h 40 min. Most of the MeOH was removed under the reduced pressure. The pH of the aqueous layer was adjusted to 2 with 1M HCl solution and extracted with EtOAc (2 x 20 mL). The organic layers were combined, dried over $MgSO_4$, filtered and the filtrate was concentrated to give 93 mg crude product. The crude product was dissolved in DMSO (4 mL), filtered through a 0.45 μm acrodisc, and purified by reverse phase HPLC (YMC C18 S-5 μm/12 nm 50 x 20 mm preparatory column), eluting at 20 mL/min with a linear gradient running from 10% CH_3CN/H_2O (0.1% TFA) to 90% CH_3CN/H_2O (0.1% TFA) over 10 min. The desired fractions were concentrated under a stream of nitrogen at 50 °C, giving 55 mg (69%) of the title compound **18**. LCMS *m/z* 505.1 $(M+H)^+$, 1.06 min (ret. time). ^1H NMR ($CDCl_3$) 7.95 (s, 1 H); 7.51 (d, *J*=1.76 Hz, 1 H); 7.42 - 7.47 (m, 1 H); 7.35 - 7.40 (m, 1 H); 7.26 - 7.31 (m, 1 H); 7.08 (dd, *J*=8.28, 2.01 Hz, 1 H); 4.74 (t, *J*=7.91 Hz, 1 H); 4.50 (s, 2 H); 4.26 (s, 3 H); 3.10 - 3.24 (m, 2 H); 2.99 (tt, *J*=12.02, 3.29 Hz, 1 H); 2.81 (s, 3 H); 2.14 (d, *J*=11.80 Hz, 2 H); 1.90 (d, *J*=11.29 Hz, 2 H); 1.72 (d, *J*=8.28 Hz, 1 H); 1.52 - 1.65 (m, 2 H); 1.17 - 1.35 (m, 3 H).

3-(1-Methyl-1*H*-1,2,3-benzotriazol-5-yl)-3-{4-methyl-3-[(*N*-methylbenzenesulfonamido)methyl]phenyl}propanoic acid (19)

To a solution of methyl 3-(3-(hydroxymethyl)-4-methyl-phenyl)-3-(1-methyl-1*H*-benzo[d][1,2,3]triazol-5-yl)propanoate **51** (123 mg, 0.36 mmol), *N*-methylbenzenesulfonamide (62 mg, 0.36 mmol) and ADDP (183 mg, 0.73 mmol) under nitrogen in THF (4 mL) stirred at 0 °C was added tributylphosphine (0.18 mL, 0.73 mmol). The reaction mixture was stirred at 0 °C for 40 min, then ambient temperature for 3 h, then treated with NaOH (2M aq. 10 mL). The mixture was stirred for a further 3 hours at room temperature, then acidified with citric acid (5% aq.) and extracted with EtOAc (x3). The combined organic layers were washed with water, brine and dried over $MgSO_4$. The product was filtered and concentrated to dryness in vacuo. The residue was purified by preparative HPLC to yield 3-(1-methyl-1*H*-1,2,3-benzotriazol-5-yl)-3-{4-methyl-3-[(*N*-methylbenzenesulfonamido)methyl]phenyl}propanoic acid **19** as a colourless oil (40 mg, 23%). ^{1}H NMR (Me-d_3-OD): 7.91-7.82 (m, 3H), 7.74-7.60 (m, 4H), 7.46 (d, J = 8.6, 1H), 7.21-7.10 (m, 3H), 4.67 (t, J = 7.8, 1H), 4.29 (s, 3H), 4.13 (s, 2H), 3.01 (d, J = 7.9, 2H), 2.46 (s, 3H), 2.40-2.30 (m, 3H). LCMS (Basic_RR01): *m/z* 479 $[M+H]^+$, RT = 1.06 min.

3-(7-Methoxy-1-methyl-1*H*-1,2,3-benzotriazol-5-yl)-3-{4-methyl-3-[(*N*-methylbenzenesulfonamido)methyl]phenyl}propanoic acid (20)

1,1'-Azodicarbonyldipiperidine (153 mg) and tri-tert¬-butyl phosphine (100 µL) were added to a solution of *N*-methylphenylsulfonamide (52 mg) and ethyl 3-[3-(hydroxymethyl)-4-methylphenyl]-3-(7-methoxy-1-methyl-1H-1,2,3-benzotriazol-5-yl)propanoate **53** (116 mg) (Davies *et al*[36], compound 29). The resulting mixture was stirred at room temperature for 3 hours. Lithium hydroxide (3 mL of a 1M solution) was added and the mixture was stirred overnight. The reaction mixture was partitioned between water and ethyl acetate. The aqueous

fraction was adjusted to pH 5 with 1M HCl and extracted with DCM (3x 10 mL). The combined organic fractions were dried over $MgSO_4$, filtered and concentrated and the residue purified by preparative HPLC to give 3-(7-methoxy-1-methyl-1*H*-1,2,3-benzotriazol-5-yl)-3-{4-methyl-3-[(*N*-methylbenzenesulfonamido)methyl]phenyl}propanoic acid **20** (39 mg, 26%). 1H NMR (Me-d_3-OD): 7.84 (2H, d), 7.73-7.55 (3H, m), 7.36 (1H, s), 7.27-7.15 (2H, m), 7.12 (1H, d), 6.83 (1H, s), 4.64 (1H, t), 4.37 (3H, s), 4.11 (2H, s), 3.93 (3H, s), 3.01-2.84 (2H, m), 2.48 (3H, s), 2.33 (3H, s). LCMS [M+H]+ 509.

3-(3-((1,1-Dioxido-3,4-dihydro-2*H*-benzo[b][1,4,5]oxathiazepin-2-yl)methyl)-4-methylphenyl)-3-(7-methoxy-1-methyl-1*H*-benzo[d][1,2,3]triazol-5-yl)propanoic acid (21)

To ethyl 3-(3-(hydroxymethyl)-4-methylphenyl)-3-(7-methoxy-1-methyl-1*H*benzo[d][1,2,3]triazol-5-yl)propanoate (483 mg, 1.260 mmol) **53** in THF (15mL) was added 3,4-dihydro-2H-benzo[b][1,4,5]oxathiazepine 1,1-dioxide **52** (376 mg, 1.889 mmol), (*E*)-diazene-1,2-diylbis(piperidin-1-ylmethanone) (636 mg, 2.52 mmol) and tributylphosphine (0.622 mL, 2.52 mmol) at 0 °C. After addition, the ice bath was removed and the reaction mixture was stirred at ambient temperature. After 21 h, the solution was dissolved in ethyl acetate and acetone, adsorbed onto isolute and purified via Combiflash chromatography to get ethyl 3-(3-((1,1-dioxido-3,4-dihydro-2*H*-benzo[b][1,4,5]oxathiazepin-2-yl)methyl)-4-methylphenyl)-3-(7-methoxy-1-methyl-1*H*-benzo[d][1,2,3]triazol-5-yl)propanoate (365 mg, 51%). LCMS *m/z* 565.4 $(M + H)^+$, 1.15 (ret. time).

To ethyl 3-(3-((1,1-dioxido-3,4-dihydro-2H-benzo[b][1,4,5]oxathiazepin-2-yl)methyl)-4-methylphenyl)-3-(7-methoxy-1-methyl-1H-benzo[d][1,2,3]triazol-5-yl)propanoate **53** (365 mg,0.646 mmol) dissolved in methanol (20 mL) was added sodium hydroxide (1M) (1.293 mL,1.293 mmol) and the mixture was heated *via* microwave at 100 °C for 1 h after which time

HCl 1M was added to the solution until pH~2-3, and the mixture was filtered to get 3-(3-((1,1-dioxido-3,4-dihydro-2*H*-benzo[b][1,4,5]oxathiazepin-2-yl)methyl)-4-methylphenyl)-3-(7-methoxy-1-methyl-1*H*-benzo[d][1,2,3]triazol-5-yl)propanoic acid **21** (311 mg, 90 %) as a colourless solid. MS *m/z* 537.4 $(M + H)^+$, 0.98 (ret. time); ^{1}H NMR ($CDCl_3$) 7.88 (d, *J*=7.5 Hz, 1H), 7.58 - 7.48 (m, 2H), 7.28 (br. s., 1H), 7.22 (d, *J*=7.8 Hz, 1H), 7.17 (s, 1H), 7.14 - 7.09 (m, 2H), 6.68 - 6.62 (m, 1H), 4.62 (t, *J*=7.9 Hz, 1H), 4.45 (s, 3H), 4.16 (br s, 4H), 3.94 (s, 3H), 3.51 (br s, 2H), 3.19 - 3.08 (m, 2H), 2.31 (s, 3H).

3-(7-Methoxy-1-methyl-1*H*-benzo[d][1,2,3]triazol-5-yl)-3-(4-methyl-3-((5-methyl-1,1-dioxido-4,5-dihydrobenzo[f][1,2,5]thiadiazepin-2(3*H*)-yl)methyl)phenyl)propanoic acid (22)

To a solution of ethyl 3-(3-(hydroxymethyl)-4-methylphenyl)-3-(7-methoxy-1-methyl-1*H*-benzo[d][1,2,3]triazol-5-yl)propanoate **53** (77 mg, 0.2 mmol) in THF (2 mL) was added 5-methyl-2,3,4,5-tetrahydrobenzo[f][1,2,5]thiadiazepine 1,1-dioxide (63.7 mg, 0.300 mmol), PS-PPh_3 (136 mg, 0.300 mmol) and DIAD (0.058 mL, 0.300 mmol). The resulting reaction mixture was stirred at ambient temperature for 160 min before adding additional PS-PPh_3 (45.5 mg, 0.100 mmol) and DIAD (0.019 mL, 0.100 mmol) and then stirred at ambient temperature for 15 min. The reaction mixture was then filtered, concentrated under reduced pressure, purified by silica gel chromatography to afford desired intermediate ethyl 3-(7-methoxy-1-methyl-1H-benzo[d][1,2,3]triazol-5-yl)-3-(4-methyl-3-((5-methyl-1,1-dioxido-4,5-dihydrobenzo[f][1,2,5]thiadiazepin-2(3H)-yl)methyl)phenyl)propanoate (43.6 mg, 38%). This intermediate was re-dissolved in MeOH (2 mL) then NaOH (2M) (0.500 mL, 1.000 mmol) was added. The resulting reaction mixture was heated with microwave irradiation at 100 °C for 1 h. The reaction mixture was acidified with HCl (1M) to pH ~3, concentrated under reduced pressure, purified with reverse phase HPLC to afford the desired product 3-(7-methoxy-1-methyl-1*H*-benzo[d][1,2,3]triazol-5-yl)-3-(4-methyl-3-((5-methyl-1,1-dioxido-4,5-

dihydrobenzo[f][1,2,5]thiadiazepin-2(3*H*)-yl)methyl)phenyl)propanoic acid **22** (37.6 mg, 34.2%). LCMS *m/z* 550 $(M + H)^+$, 0.98 (ret. time). ^{1}H NMR (Me-d_3-OD) 7.85 (dd, *J*=1.5, 8.0 Hz, 1H), 7.55 - 7.47 (m, 1H), 7.39 (s, 1H), 7.27 (s, 1H), 7.19 (d, *J*=8.0 Hz, 2H), 7.16 - 7.11 (m, 1H), 7.06 (t, *J*=7.7 Hz, 1H), 6.83 (s, 1H), 4.62 (t, *J*=7.9 Hz, 1H), 4.41 (s, 3H), 4.19 (s, 2H), 3.96 (s, 3H), 3.27 (s, 4H), 3.12 (dd, *J*=3.6, 7.9 Hz, 2H), 3.01 (s, 3H), 2.30 (s, 3H).

3-(7-Methoxy-1-methyl-1*H*-benzo[d][1,2,3]triazol-5-yl)-3-(4-methyl-3-((3-methyl-1,1-dioxido-3,4-dihydro-2*H*-benzo[b][1,4,5]oxathiazepin-2-yl)methyl)phenyl)propanoic acid (23)

To a solution of ethyl 3-(3-(hydroxymethyl)-4-methylphenyl)-3-(7-methoxy-1-methyl-1*H*-benzo[d][1,2,3]triazol-5-yl)propanoate **53** (77 mg, 0.2 mmol) in THF (2 mL) was added 3-methyl-3,4-dihydro-2*H*-benzo[b][1,4,5]oxathiazepine 1,1-dioxide **60** (64.0 mg, 0.300 mmol), PS-PPh_3 (136 mg, 0.300 mmol) and DIAD (0.058 mL, 0.300 mmol). The resulting reaction mixture was stirred at ambient temperature for 92 h. To this reaction mixture was added more PS-PPh_3 (45.5 mg, 0.100 mmol) and DIAD (0.019 mL, 0.100 mmol) and the mixture stirred at ambient temperature for 90 min. To the reaction mixture was added more PS-PPh_3 (136 mg, 0.300 mmol) and DIAD (0.058 mL, 0.300 mmol) and the mixture stirred at ambient temperature for 35 min. The reaction mixture was filtered, concentrated under reduced pressure to afford desired intermediate ethyl 3-(7-methoxy-1-methyl-1*H*-benzo[d][1,2,3]triazol-5-yl)-3-(4-methyl-3-((3-methyl-1,1-dioxido-3,4-dihydro-2*H*-benzo[b][1,4,5]oxathiazepin-2-yl)methyl)phenyl)propanoate (**61**). This intermediate was re-dissolved in MeOH (2.000 mL) after which time NaOH (2M) (0.500 mL, 1.000 mmol) was added. The resulting reaction mixture was heated with microwave irradiation at 100 °C for 30 min. The reaction mixture was acidified with HCl (1M) to pH ~3, evaporated under vacuum, and purified via reverse phase HPLC to afford the desired product 3-(7-methoxy-1-methyl-1*H*-benzo[d][1,2,3]triazol-5-yl)-

3-(4-methyl-3-((3-methyl-1,1-dioxido-3,4-dihydro-2*H*-benzo[b][1,4,5]oxathiazepin-2-yl)methyl)phenyl)propanoic acid **23** (62.1 mg, 56.4%). LCMS *m/z* 551 $(M + H)^+$, 1.07 (ret. time). ^{1}H NMR ($CDCl_3$) 7.83 (d, *J*=7.8 Hz, 1H), 7.45 (d, *J*=7.5 Hz, 4H), 7.18 (t, *J*=7.5 Hz, 1H), 7.14 - 7.04 (m, 3H), 6.66 (s, 1H), 4.67 - 4.48 (m, 2H), 4.47 - 4.37 (m, 4H), 4.25 (td, *J*=4.5, 13.1 Hz, 1H), 4.08 (dd, *J*=8.8, 15.3 Hz, 1H), 3.94 (s, 4H), 3.21 - 3.07 (m, 2H), 2.26 (s, 3H), 1.07 - 0.96 (m, 3H).

3-(7-Methoxy-1-methyl-1*H*-benzo[d][1,2,3]triazol-5-yl)-3-(4-methyl-3-((4-methyl-1,1-dioxido-3,4-dihydro-2*H*-benzo[b][1,4,5]oxathiazepin-2-yl)methyl)phenyl)propanoic acid (24)

To a solution of ethyl 3-(3-(hydroxymethyl)-4-methylphenyl)-3-(7-methoxy-1-methyl-1H-benzo[d][1,2,3]triazol-5-yl)propanoate **53** (77 mg, 0.2 mmol) in THF (2 mL) was added 4-methyl-3,4-dihydro-2H-benzo[b][1,4,5]oxathiazepine 1,1-dioxide **63** (64.0 mg, 0.300 mmol), PS-PPh_3 (136 mg, 0.300 mmol) and DIAD (0.058 mL, 0.300 mmol). The resulting reaction mixture was stirred at ambient temperature for 1 h. The reaction mixture was filtered, concentrated under reduced pressure, purified by silica gel chromatography to afford desired intermediate ethyl 3-(7-methoxy-1-methyl-1H-benzo[d][1,2,3]triazol-5-yl)-3-(4-methyl-3-((4-methyl-1,1-dioxido-3,4-dihydro-2H-benzo[b][1,4,5]oxathiazepin-2-yl)methyl)phenyl)propanoate **64**. This intermediate was re dissolved in MeOH (2.000 mL) and NaOH (2M) (0.500 mL, 1.000 mmol) was added. The resulting reaction mixture was heated with microwave irradiation at 100 °C for 30 min. The reaction mixture was acidified with HCl (1M) to pH ~3, concentrated under reduced pressure, purified by reverse phase HPLC to afford the desired product 3-(7-methoxy-1-methyl-1*H*-benzo[d][1,2,3]triazol-5-yl)-3-(4-methyl-3-((4-methyl-1,1-dioxido-3,4-dihydro-2*H*-benzo[b][1,4,5]oxathiazepin-2-yl)methyl)phenyl)propanoic acid **24** (66.9 mg, 60.7%). LCMS *m/z* 551 $(M + H)^+$, 1.00 (ret.

time). ^{1}H NMR ($CDCl_3$) 9.04 (br. s., 1H), 7.85 (d, J=7.8 Hz, 1H), 7.59 - 7.45 (m, 2H), 7.26 - 7.15 (m, 3H), 7.12 (d, J=4.0 Hz, 2H), 6.66 (s, 1H), 4.61 (d, J=3.3 Hz, 1H), 4.55 - 4.42 (m, 4H), 4.25 (dd, J=5.4, 11.2 Hz, 1H), 3.94 (s, 3H), 3.84 - 3.65 (m, 2H), 3.24 - 3.05 (m, 2H), 2.92 (t, J=14.8 Hz, 1H), 2.29 (s, 3H), 1.31 - 1.15 (m, 3H).

3-(7-Methoxy-1-methyl-1*H*-benzo[d][1,2,3]triazol-5-yl)-3-(3-((4-methyl-1,1-dioxido-3,4-dihydro-2*H*-benzo[b][1,4,5]oxathiazepin-2-yl)methyl)phenyl)propanoic acid (25)

To a stirred solution of ethyl 3-(3-(hydroxymethyl)phenyl)-3-(7-methoxy-1-methyl-1H-benzo[d][1,2,3]triazol-5-yl)propanoate **66** (50 mg, 0.135 mmol) dissolved in dry THF (2 mL) was added 4-methyl-3,4-dihydro-2*H*-benzo[b][1,4,5]oxathiazepine 1,1-dioxide **63** (53.3 mg, 0.249 mmol), DIAD (0.088 mL, 0.400 mmol) and PS-PPh_3 (169 mg, 0.271 mmol) at 0 °C. The ice bath was removed after 20 min, and the mixture was stirred at ambient temperature for 50 h. The mixture was filtered, concentrated, dissolved in MeOH (2 mL); then NaOH 1M (1.088 mL, 1.088 mmol) was added and the mixture was heated via microwave for 2 h at 100 °C (after 1 h 34-10). The resulting mixture was acidified with HCl 6M (182 mL) then HCl 1M was added until pH 2. The resulting mixture was concentrated under reduced pressure and purified on reverse-phase HPLC (Sunfire C18, 19x100mm, 5u column), eluting at 18 mL/min with a linear gradient running from 35% CH_3CN/H_2O (0.1% formic acid) to 65% CH_3CN/H_2O (0.1% formic acid) over 10 min. The desired fractions were collected and dried by V10 solvent evaporator. Dried fractions were transferred to a vial with MeCN, and dried under N_2 stream at 45 °C then evaporated down and purified via reverse phase HPLC using a Sunfire C18, 19x100mm, 5u column, eluting with water containing 0.1% formic acid (A) and MeCN containing 0.1% formic acid (B) with a gradient of 35% B to 65% B in 10 min at a flow rate of 18 mL/min to get 3-(7-methoxy-1-methyl-1*H*-benzo[d][1,2,3]triazol-5-yl)-3-(3-((4-methyl-1,1-dioxido-3,4-dihydro-2*H*-benzo[b][1,4,5]oxathiazepin-2-yl)methyl)phenyl)propanoic acid

25 (27.7 mg, 38 %). LCMS *m/z* 537.2 $(M+H)^+$, 0.98 (ret. time). ^{1}H NMR ($CDCl_3$) 7.86 (d, J=7.8 Hz, 1H), 7.57 - 7.43 (m, 2H), 7.32 - 7.28 (m, 1H), 7.26 - 7.14 (m, 5H), 6.67 - 6.56 (m, 1H), 4.64 (br. s., 1H), 4.53 - 4.40 (m, 4H), 4.23 (br. s., 1H), 3.96 - 3.72 (m, 5H), 3.23 - 3.00 (m, 3H), 1.36 - 1.26 (m, 3H).

3-(7-Methoxy-1-methyl-1*H*-benzo[d][1,2,3]triazol-5-yl)-3-(4-methyl-3-(((*R*)-4-methyl-1,1-dioxido-3,4-dihydro-2*H*-benzo[b][1,4,5]oxathiazepin-2-yl)methyl)phenyl)propanoic acid (26)

To a solution of ethyl 3-(3-(hydroxymethyl)-4-methylphenyl)-3-(7-methoxy-1-methyl-1H-benzo[d][1,2,3]triazol-5-yl)propanoate **53** (100 mg, 0.261 mmol) in THF (4 mL) was added (*R*)-4-methyl-3,4-dihydro-2H-benzo[b][1,4,5]oxathiazepine 1,1-dioxide (83 mg, 0.391 mmol), PS-PPh_3 (237 mg, 0.522 mmol) and DIAD (0.101 mL, 0.522 mmol). The resulting reaction mixture was stirred at ambient temperature for 25 min. The reaction mixture was filtered and the filtrate was concentrated to afford desired crude intermediate ethyl 3-(7-methoxy-1-methyl-1*H*-benzo[d][1,2,3]triazol-5-yl)-3-(4-methyl-3-(((*R*)-4-methyl-1,1-dioxido-3,4-dihydro-2*H*-benzo[b][1,4,5]oxathiazepin-2-yl)methyl)phenyl)propanoate. To this intermediate was added MeOH (4 mL) and NaOH (2M) (0.652 mL, 1.304 mmol). The resulting reaction mixture was heated with microwave irradiation at 80 °C for 30 min. The reaction mixture was acidified with HCl (1M) to pH ~3, concentrated under reduced pressure, purified by reverse phase HPLC to afford the desired product 3-(7-methoxy-1-methyl-1*H*-benzo[d][1,2,3]triazol-5-yl)-3-(4-methyl-3-(((*R*)-4-methyl-1,1-dioxido-3,4-dihydro-2*H*-benzo[b][1,4,5]oxathiazepin-2-yl)methyl)phenyl)propanoic acid **26** (58.1 mg, 40.5%). LCMS *m/z* 551 $(M + H)^+$, 0.98 (ret. time). ^{1}H NMR ($CDCl_3$) 7.86 (d, J=7.5 Hz, 1H), 7.56 - 7.43 (m, 2H), 7.26 - 7.15 (m, 2H), 7.11 (s, 3H), 6.56 (br. s., 1H), 4.64 - 4.49 (m, 2H), 4.39 (s, 3H), 4.22 (br. s., 1H), 3.89 (s, 3H), 3.84 - 3.64 (m, 2H), 3.20 - 3.02 (m, 2H), 2.89 (t, J=14.4 Hz, 1H), 2.30 (s, 3H), 1.26 - 1.12 (m, 3H).

3-(7-Methoxy-1-methyl-1*H*-benzo[d][1,2,3]triazol-5-yl)-3-(4-methyl-3-(((*S*)-4-methyl-1,1-dioxido-3,4-dihydro-2H-benzo[b][1,4,5]oxathiazepin-2-yl)methyl)phenyl)propanoic acid (27)

To a solution of ethyl 3-(3-(hydroxymethyl)-4-methylphenyl)-3-(7-methoxy-1-methyl-1*H*-benzo[d][1,2,3]triazol-5-yl)propanoate **53** (100 mg, 0.261 mmol) in THF (4 mL) was added (*S*)-4-methyl-3,4-dihydro-2*H*-benzo[b][1,4,5]oxathiazepine 1,1-dioxide (83 mg, 0.391 mmol), PS-PPh_3 (237 mg, 0.522 mmol) and DIAD (0.101 mL, 0.522 mmol). The resulting reaction mixture was stirred at ambient temperature for 25 min. The reaction mixture was filtered and the filtrate was concentrated to afford desired crude intermediate ethyl 3-(7-methoxy-1-methyl-1H-benzo[d][1,2,3]triazol-5-yl)-3-(4-methyl-3-(((S)-4-methyl-1,1-dioxido-3,4-dihydro-2H-benzo[b][1,4,5]oxathiazepin-2-yl)methyl)phenyl)propanoate. To this intermediate was added MeOH (4 mL) then NaOH (2M) (0.652 mL, 1.304 mmol). The resulting reaction mixture was heated with microwave irradiation at 80 °C for 30 min. The reaction mixture was acidified with HCl (1M) to pH ~3, concentrated under reduced pressure, purified by reverse phase HPLC to afford the desired product 3-(7-methoxy-1-methyl-1*H*-benzo[d][1,2,3]triazol-5-yl)-3-(4-methyl-3-(((*S*)-4-methyl-1,1-dioxido-3,4-dihydro-2*H*-benzo[b][1,4,5]oxathiazepin-2-yl)methyl)phenyl)propanoic acid **27** (37.2 mg, 25.9%). LCMS *m/z* 551 $(M + H)^+$, 0.97 (ret. time). ^{1}H NMR ($CDCl_3$) 7.88 (d, *J*=7.5 Hz, 1H), 7.57 - 7.44 (m, 2H), 7.28 - 7.23 (m, 1H), 7.20 (dd, *J*=3.4, 7.7 Hz, 1H), 7.13 (s, 3H), 6.58 (d, *J*=2.3 Hz, 1H), 4.66 - 4.51 (m, 2H), 4.41 (s, 3H), 4.29 - 4.18 (m, 1H), 3.91 (s, 3H), 3.83 - 3.67 (m, 2H), 3.21 - 3.04 (m, 2H), 2.91 (t, *J*=14.6 Hz, 1H), 2.32 (s, 3H), 1.26 - 1.16 (m, 3H).

(3*R*)-3-(7-Methoxy-1-methyl-1*H*-benzo[d][1,2,3]triazol-5-yl)-3-(4-methyl-3-(((*R*)-4-methyl-1,1-dioxido-3,4-dihydro-2*H*-benzo[b][1,4,5]oxathiazepin-2-yl)methyl)phenyl)propanoic acid (28)

To a solution of ethyl 3-(3-(hydroxymethyl)-4-methylphenyl)-3-(7-methoxy-1-methyl-1*H*-benzo[d][1,2,3]triazol-5-yl)propanoate **53** (980 mg, 2.56 mmol) in THF (30 mL) was added (*R*)-4-methyl-3,4-dihydro-2*H*-benzo[b][1,4,5]oxathiazepine 1,1-dioxide (818 mg, 3.83 mmol), PS-PPh_3 (3195 mg, 5.11 mmol) and then DIAD (0.994 mL, 5.11 mmol) in THF (10 mL). The resulting reaction mixture was stirred at ambient temperature for 30 min. The reaction mixture was filtered and the filtrate was concentrated under reduced pressure, purified via flash chromatography over silica gel to afford the desired crude intermediate ethyl 3-(7-methoxy-1-methyl-1H-benzo[d][1,2,3]triazol-5-yl)-3-(4-methyl-3-(((R)-4-methyl-1,1-dioxido-3,4-dihydro-2H-benzo[b][1,4,5]oxathiazepin-2-yl)methyl)phenyl)propanoate (1.2990 g, 88%). This crude intermediate was dissolved in MeOH (30.0 mL) then NaOH (2M) (6.39 mL, 12.78 mmol) was added. The resulting reaction mixture was stirred at 80 °C for 40 min. The reaction mixture was acidified with HCl (1M) to pH ~3, concentrated under reduced pressure, and extracted with EtOAc (3 x 50 mL). The combined organic layer was washed with brine (50 mL), dried over $MgSO_4$, filtered, and concentrated under reduced pressure to afford the desired product 3-(7-methoxy-1-methyl-1H-benzo[d][1,2,3]triazol-5-yl)-3-(4-methyl-3-(((R)-4-methyl-1,1-dioxido-3,4-dihydro-2H-benzo[b][1,4,5]oxathiazepin-2-yl)methyl)phenyl)propanoic acid (1.4075 g, 100%). This was purified via reverse phase HPLC using a Sunfire C18, 19x100mm, 5u column, eluting with water containing 0.1% formic acid (A) and MeCN containing 0.1% formic acid (B) with a gradient of 35% B to 65% B in 10 min at a flow rate of 18 mL/min. The title compound was then obtained by SFC chiral purification using a ChiralAD, 21x250mm, 5u column with 25% MeOH:IPA (1:1) as eluent at 55 g/min flow rate and a back pressure of 100 bar to obtain 400 mg, 28.4% of the title compound **28**.

LCMS *m/z* 551 $(M + H)^+$, 1.02 (ret. time). ^{1}H NMR ($CDCl_3$) 7.86 (dd, *J*=1.5, 7.8 Hz, 1H), 7.51 (dt, *J*=1.6, 7.7 Hz, 1H), 7.46 (s, 1H), 7.24 (dt, *J*=1.0, 7.5 Hz, 1H), 7.19 (d, *J*=8.0 Hz, 1H), 7.15 - 7.08 (m, 3H), 6.55 (s, 1H), 4.61 (t, *J*=7.9 Hz, 1H), 4.54 (d, *J*=14.1 Hz, 1H), 4.40 (s, 3H), 4.29 - 4.19 (m, 1H), 3.89 (s, 3H), 3.82 - 3.66 (m, 2H), 3.20 - 3.03 (m, 2H), 2.94 - 2.86 (m, 1H), 2.31 (s, 3H), 1.23 - 1.21 (m, 3H).

3-(4-Chlorobenzoyl)phenol (31)

A solution of 3-(2-tetrahydro-2*H*-pyranoxy)phenylmagnesium bromide (**30**) in THF (0.5M, 12.6 mL, 3.32 mmol) was added to neat 4-chlorobenzonitrile (0.435 mg, 3.16 mmol) under N_2. The reaction mixture was refluxed for 6 hours at 75 °C. The solution was then transferred into a mixture of concentrated aqueous HCl (4 mL) and ice. The mixture was warmed to room temperature and stirred for 1 hour. The product was extracted with EtOAc (x3) and the combined organic layers were washed with water then brine before being dried with anhydrous $MgSO_4$. The filtrate was concentrated to dryness in vacuo. The resulting solid was triturated with $CHCl_3$ and filtered to yield 3-(4-chlorobenzoyl)phenol **31** (335 mg, 45%) as a pale yellow solid. More product was contained in the filtrate. ^{1}H NMR (DMSO-d_6): 9.89 (s, 1H), 7.80-7.69 (m, 2H), 7.67-7.61 (m, 2H), 7.37 (t, *J* = 7.8 Hz, 1H), 7.16-7.04 (m, 3H). LCMS (Acidic_RR02): *m/z* 233 $[M+H]^+$, RT = 1.36 min. Purity >95%.

Methyl 3-(4-chlorophenyl)-3-(3-methoxyphenyl)propanoate (32)

A solution of ^{t}BuOK (222 mg, 1.98 mmol) in THF (9 mL) under N_2 at 0 °C was treated with trimethyl phosphonoacetate (355 µL, 2.15 mmol). After 10 mins, 3-(4-chlorobenzoyl)phenol **31** (200 mg, 0.86 mmol) was added slowly. The mixture became a bright yellow suspension and was stirred for 4 hours, while being allowed to warm to room temperature. The reaction was then quenched with NH_4Cl (aq., sat.), diluted with water and then extracted with *n*-heptane

(x3). The combined organic layers were washed with water and brine and dried over $MgSO_4$. The product was filtered and concentrated to dryness in vacuo to yield methyl 3-(4-chlorophenyl)-3-(3-methoxyphenyl)prop-2-enoate (200 mg, 69%) as a pale yellow solid. LCMS (Acidic_RR02): *m/z* 303 $[M+H]^+$, RT = 1.58 min. Purity >85%. A solution of methyl 3-(4-chlorophenyl)-3-(3-methoxyphenyl)prop-2-enoate (200 mg, 0.59 mmol) in MeOH (10.0 mL) under N_2 was treated with $NiCl_2.6H_2O$ (28 mg, 0.12 mmol). The reaction was cooled to 0 °C and sodium borohydride (67 mg 1.78 mmol) was added slowly in portions. The mixture became black and effervescence observed. After the reaction mixture was stirred for 16 h at room temperature, the reaction was quenched with NH_4Cl (sat., aq.) and diluted with EtOAc. The organic layer was separated and dried over $MgSO_4$, filtrated and concentrated to dryness under reduced pressure. The product was purified by column chromatography to yield methyl 3-(4-chlorophenyl)-3-(3-methoxyphenyl)propanoate **32** (157 mg) as a colourless oil. ^{1}H NMR (Me-d_3-OD): 7.33-7.24 (m, 4H), 7.23-7.16 (m, 1H), 6.89-6.73 (m, 3H), 4.49 (t, J = 8.0 Hz, 1H), 3.76 (s, 3H), 3.58 (s, 3H), 3.08 (d, J = 8.1 Hz, 2H).

_N_-Methoxy-_N_-methyl-[1,2,4]triazolo[4,3-a]pyridine-7-carboxamide (36)

To [1,2,4]-triazolo[4,3-a]pyridine-7-carboxylic acid **35** (250 mg, 1.53 mmol) and *N*,*O*-dimethylhydroxylamine hydrochloride (229 mg, 2.30 mmol) in DCM (7.7 mL) was added *N*-methylmorpholine (758 µl, 6.90 mmol) and HBTU (890 mg, 2.30 mmol). DMF (3 mL) was added for solubility. The reaction was stirred at room temperature for 3 hours and then quenched by adding $NaHCO_3$ (sat., aq.). The product was extracted with $CHCl_3$ (x3). The combined organic layers were washed with water, brine and dried over $MgSO_4$. The product was filtered and evaporated in vacuo to yield *N*-methoxy-*N*-methyl-[1,2,4]triazolo[4,3-a]pyridine-7-carboxamide **36** (148 mg, 47%) taken on as is. ^{1}H NMR (Me-d_3-OD): 9.27 (d, J = 1.1 Hz, 1H), 8.57 (dd, J = 7.1, 1.2 Hz, 1H), 8.11-8.08 (m, 1H), 7.25 (dd, J = 7.1, 1.5 Hz, 1H),

3.68 (s, 3H), 3.43 (s, 3H). LCMS (Acidic_RR02): *m/z* 207 $[M+H]^+$, RT = 0.24 min. Purity >80%.

7-(4-Chlorobenzoyl)-[1,2,4]triazolo[4,3-a]pyridine (37)

To a solution of *N*-methoxy-*N*-methyl-[1,2,4]triazolo[4,3-a]pyridine-7-carboxamide **36** (148 mg, 0.72 mmol) in THF (7 mL) was added 4-chlorophenylmagnesium bromide (1M THF) (860 µL, 0.86 mmol) at 0 °C, under N_2. The reaction was allowed to warm to room temperature over 1 hour, and was quenched with NH_4Cl (sat., aq.). The product was extracted with EtOAc, which was washed with water, then with brine, and dried over $MgSO_4$. The product was filtered and evaporated in vacuo to yield 7-(4-chlorobenzoyl)-[1,2,4]triazolo[4,3-a]pyridine **37** (118 mg, 64%) as a pale yellow solid. Taken on as is. ^{1}H NMR (Me-d_3-OD): 9.34 (d, J = 1.0 Hz, 1H), 8.64 (dd, J = 7.1, 1.1 Hz, 1H), 8.12-8.09 (m, 1H), 7.94-7.89 (m, 2H), 7.65-7.60 (m, 2H), 7.41 (dd, J = 7.2, 1.6 Hz, 1H). LCMS (Acidic_RR02): *m/z* 258 $[M+H]^+$, RT = 1.15 min. Purity >85%.

Methyl 3-(4-chlorophenyl)-3-{[1,2,4]triazolo[4,3-a]pyridin-7-yl}prop-2-enoate (38)

To a solution of ^{t}BuOK (154 mg, 1.37 mmol) in THF (5 mL) at 0 °C, was added trimethyl phosphonoacetate (174 µL, 1.05 mmol), under N_2. A colourless precipitate formed. After 10 minutes, the 7-(4-chlorobenzoyl)-[1,2,4]triazolo[4,3-a]pyridine **37** (118 mg, 0.46 mmol) was added slowly. The reaction was stirred for 20 hours at room temperature and then quenched with NH_4Cl (aq., sat.). The mixture was diluted with water and the product extracted with *n*-heptane (x3). The combined organic layers were washed with water and brine and dried over $MgSO_4$. The product was filtered, evaporated in vacuo and purified by column chromatography to yield methyl 3-(4-chlorophenyl)-3-{[1,2,4]triazolo[4,3-a]pyridin-7-yl}prop-2-enoate **38** (144 mg) as a yellow oil. ^{1}H NMR (Me-d_3-OD): 9.24 (0.6H, s), 9.20 (0.4H, s), 8.53 (0.6H, dd),

8.49 (0.4H, dd), 7.60 (0.6H, s), 7.49-7.42 (2.8H, m), 7.29-7.24 (0.6H, m), 7.15 (0.4H, dd), 6.85 (0.6H, dd), 6.73 (0.4H, s), 6.63 (0.6H, s), 3.66 (1.8H, s), 3.65 (1.2H, s). Two alkene isomers ~2:1. LCMS (Acidic_RR02): *m/z* 314 $[M+H]^+$, RT = 1.22 and 1.25 min. Purity >85%.

6-Bromo-3-methyl-1,2-benzisoxazole (40)

6-Bromo-3-methyl-1,2-benzisoxazole was prepared according to the method of Chen *et al*[39]. ^{1}H NMR (Me-d_3-OD): 7.86 (1H, d), 7.71 (1H, d), 7.53 (1H, dd), 2.59 (3H, s).

3-Methyl-6-(4,4,5,5-tetramethyl-1,3,2-dioxaborolan-2-yl)-1,2-benzoxazole (41)

A solution of 6-bromo-3-methyl-1,2-benzisoxazole **40** (217 mg, 1.02 mmol), bispinacolato diboron (286 mg, 1.13 mmol) and potassium acetate (201 mg, 2.05 mmol) in 1,4-dioxane (10 mL) was degassed by bubbling through nitrogen for 10 minutes. $PdCl_2$dppf (37 mg, 0.05 mmol) was added and the mixture was heated to 90 °C for 2 hours. The reaction was cooled and the mixture partitioned between water (20 mL) and ethyl acetate (3 x 20 mL). The combined organic fractions were dried over $MgSO_4$, filtered and concentrated. The residue was columned in 0-30% ethyl acetate and petrol to give 3-methyl-6-(4,4,5,5-tetramethyl-1,3,2-dioxaborolan-2-yl)-1,2-benzoxazole **41** (202 mg, 76%). LCMS $[M+H]^+$ 260.

***N*-Methylpyridine-3-sulfonamide (45)**

A solution of 3-pyridyl sulfonyl chloride **44** (355 mg) in DCM (3 mL) was cooled to 0 °C. Methyl amine (3 mL of a 33% by weight solution in THF) was added and the reaction stirred 30 min. The reaction was concentrated. The residue was taken up in DCM (10 mL) and washed with saturated aqueous $NaHCO_3$. The organic layer was dried over $MgSO_4$, filtered and

concentrated to give *N*-methylpyridine-3-sulfonamide **45** (257 mg) as a white solid which was used without further purification.

_N_,1,5-Trimethyl-1_H_-pyrazole-4-sulfonamide (47)

A solution of 1,5-dimethyl-1*H*-pyrazole-4-sulfonyl chloride (389 mg) in DCM (3 mL) was cooled to 0 °C. Methyl amine (3 mL of a 33% by weight solution in THF) was added and the reaction stirred 30 min. The reaction was filtered and the liquor concentrated to give *N*,1,5-trimethyl-1*H*-pyrazole-4-sulfonamide **47** (312 mg) which was used without further purification.

_N_-Methylcyclohexanesulfonamide (49)

Methylamine (2.0 M in THF) (2.5 mL, 5 mmol) was added to a solution of cyclohexanesulfonyl chloride (0.40 mL, 2.46 mmol) in dichloromethane (5 mL) at 0 °C. The solution was stirred for 20 h. The mixture was diluted with DCM and washed with 10% $NaHCO_3$ solution and brine. The organic layer was dried via $MgSO_4$, filtered and the filtrate was concentrated under reduced pressure to give 380 mg (87%) of the title compound **49**. LCMS *m/z* 177.9 $(M+H)^+$, 0.57 min (ret. time).

Methyl 3-(4-chloro-3-((_N_-methylcyclohexanesulfonamido)methyl)phenyl)-3-(1-methyl-1_H_-benzo[d][1,2,3]triazol-5-yl)propanoate (50)

To a solution of methyl 3-(4-chloro-3-(hydroxymethyl)phenyl)-3-(1-methyl-1*H*-benzo[d][1,2,3]triazol-5-yl)propanoate **46** (137 mg, 0.38 mmol), *N*-methylcyclohexanesulfonamide **49** (183 mg, 1.03 mmol) and ADDP (207 mg, 0.82 mmol) under nitrogen in THF (5 mL) stirred at 0 °C was added tributylphosphine (0.2 mL, 0.81 mmol). The reaction mixture was stirred at 0 °C for 40 min, during which a precipitate was generated.

The mixture was stirred at ambient temperature for 66 h. Most solvent was removed under reduced pressure, the residue was dissolved in EtOAc, washed with brine and dried with $MgSO_4$. The mixture was filtered and the filtrate was adsorbed onto isolute and purified by silica gel chromatography (Combiflash, 12 g), eluting at 20 mL/min with a gradient running from 100% hexane to 80% EtOAc/hexane over 35 min. Product containing fractions were combined and concentrated to give 82 mg (42%) of the title compound **50**. LCMS *m/z* 519.1 $(M+H)^+$, 1.16 min (ret. time).

Methyl 3-(3-(hydroxymethyl)-4-methyl-phenyl)-3-(1-methyl-1*H*-benzo[d][1,2,3]triazol-5-yl)propanoate (51)

A stirred solution of (*E*)-Methyl 3-(1-methyl-1*H*-benzo[d][1,2,3]triazol-5-yl)acrylate **43** (Davies *et al*[36], compound 19) (325 mg, 1.50 mmol) in 1,4-dioxane (5 mL) /water (0.5 mL) was treated with 3-(hydroxymethyl)-4-methyl-phenylboronic acid (498 mg, 3.00 mmol), Et_3N (0.30 mL, 2.25 mmol) and $[RhCl(cod)]_2$ (37 mg, 0.08 mmol). After purging with N_2 for 10 min, the mixture was stirred at 95 °C for 3 h, then cooled and partitioned between EtOAc and water. The aqueous phase was extracted with EtOAc (2x) and the combined organic phases dried ($MgSO_4$), filtered and concentrated to dryness. The residue was purified using silica chromatography (EtOAc/petrol gradient 30-80%) to give the title compound (406 mg, 80%). LCMS $[M+H]^+$ 340.

2-((2-Hydroxyethyl)(methyl)amino)benzenesulfonamide (55)

A solution of 2-fluorobenzenesulfonamide **54** (2.102 g, 12 mmol) in 2-(methylamino)ethanol (9.64 mL, 120 mmol) was heated with microwave irradiation at 130 °C for 30 min then heated again with microwave at 130 °C for 30 min. The reaction mixture was diluted with H_2O (100 mL), adjusted pH to ~5 with HCl (6M then 1M), extracted with EtOAc (3 x 100 mL). The

organic layer was washed with brine (50 mL), dried over $MgSO_4$, filtered, concentrated under reduced pressure, to afford the desired product 2-((2-hydroxyethyl)(methyl)amino)benzenesulfonamide **55** (2.4151 g, 87%). LCMS *m/z* 231 $(M + H)^+$, 0.55 (ret. time).

5-Methyl-2,3,4,5-tetrahydrobenzo[f][1,2,5]thiadiazepine 1,1-dioxide (56)

To a solution of 2-((2-hydroxyethyl)(methyl)amino)benzenesulfonamide (461 mg, 2 mmol) in THF (100 mL) was added DIAD (0.778 mL, 4.00 mmol) and PS-PPh_3 (1818 mg, 4.00 mmol). The resulting reaction mixture was stirred at ambient temperature for 17 h. The reaction mixture was filtered, concentrated under reduced pressure, purified by silica gel chromatography to afford the desired product 5-methyl-2,3,4,5-tetrahydrobenzo[f][1,2,5]thiadiazepine 1,1-dioxide **56** (310.1 mg, 73%). LCMS *m/z* 213 $(M + H)^+$, 0.59 (ret. time).

2-Fluoro-*N*-(1-hydroxypropan-2-yl)benzenesulfonamide (59)

To a solution of 2-amino-1-propanol (0.390 mL, 5.00 mmol) in THF (10 mL) and water (2 mL) was added K_2CO_3 (0.691 g, 5.00 mmol) and then 2-fluorobenzene-1-sulfonyl chloride (0.662 mL, 5 mmol) slowly. The resulting reaction mixture was stirred at ambient temperature for 17 h. The reaction mixture was diluted with H_2O (3 mL), extracted with EtOAc (2 x 10 mL). The combined organic layer was washed with brine (10 mL), dried over $MgSO_4$, filtered, and concentrated under reduced pressure to afford the desired product 2-fluoro-*N*-(1-hydroxypropan-2-yl)benzenesulfonamide **59** (1.2145 g, 104%). LCMS *m/z* 234 $(M + H)^+$, 0.57 (ret. time).

3-Methyl-3,4-dihydro-2*H*-benzo[b][1,4,5]oxathiazepine 1,1-dioxide (60)

To a solution of 2-fluoro-N-(1-hydroxypropan-2-yl)benzenesulfonamide (1.166 g, 5 mmol) in DMSO (20 mL) was added ^{t}BuOK (1.683 g, 15.00 mmol). The resulting reaction mixture was heated with microwave irradiation at 100 °C for 30 min. The reaction mixture was concentrated under reduced pressure, then was added H_2O (10 mL), and adjusted to pH ~7 with HCl (1M), and extracted with EtOAc (3 x 20 mL). The combined organic layer was washed with brine (20 mL), dried over $MgSO_4$, filtered, concentrated under reduced pressure, purified by silica gel chromatography to afford desired product 3-methyl-3,4-dihydro-2*H*-benzo[b][1,4,5]oxathiazepine 1,1-dioxide **60** (1.0843 g, 102%). LCMS *m/z* 214 $(M + H)^+$, 0.48 (ret. time).

2-Fluoro-*N*-(2-hydroxypropyl)benzenesulfonamide (62)

To a solution of 1-amino-2-propanol (0.386 mL, 5.00 mmol) in THF (10 mL) and water (2.5 mL) was added K_2CO_3 (0.691 g, 5.00 mmol) and then 2-fluorobenzene-1-sulfonyl chloride (0.662 mL, 5 mmol) slowly. The resulting reaction mixture was stirred at ambient temperature for 24 h. The reaction mixture was diluted with H_2O (10 mL) then extracted with EtOAc (20 + 2 x 10 mL). The combined organic layer was washed with brine (15 mL), dried over $MgSO_4$, filtered, and then concentrated under vacuum to afford the desired product 2-fluoro-*N*-(2-hydroxypropyl)benzenesulfonamide **62** (1.2272 g, 105%). LCMS *m/z* 234 $(M + H)^+$, 0.64 (ret. time).

4-Methyl-3,4-dihydro-2*H*-benzo[b][1,4,5]oxathiazepine 1,1-dioxide (63)

To a solution of 2-fluoro-N-(2-hydroxypropyl)benzenesulfonamide (1.166 g, 5 mmol) in DMSO (20 mL) was added ^{t}BuOK (1.683 g, 15.00 mmol). The resulting reaction mixture was heated with microwave irradiation at 100 °C for 30 min. The reaction mixture was diluted with

H_2O (30 mL), acidified with HCl (1M) to pH ~6 and extracted with EtOAc (3 x 50 mL). The combined organic layer was washed with brine (50 mL), dried over $MgSO_4$, filtered, concentrated under reduced pressure, purified by silica gel chromatography to afford the desired product 4-methyl-3,4-dihydro-2*H*-benzo[b][1,4,5]oxathiazepine 1,1-dioxide **63** (0.9423 g, 88%). LCMS *m/z* 214 $(M + H)^+$, 0.61 (ret. time).

Ethyl 3-(3-(hydroxymethyl)phenyl)-3-(7-methoxy-1-methyl-1*H*-benzo[d][1,2,3]triazol-5-yl)propanoate (66)

To a solution of (*E*)-ethyl 3-(7-methoxy-1-methyl-1*H*-benzo[d][1,2,3]triazol-5-yl)acrylate (**65**[36]**,** (1 g, 3.83 mmol) dissolved in 1,4-dioxane (10 mL) and water (10 mL) was added (3-(hydroxymethyl)phenyl)boronic acid (1.90 g, 12.50 mmol), $[RhCl(cod)]_2$ (0.423 g, 0.765 mmol) and TEA (1.227 mL, 8.80 mmol) and the mixture was heated *via* microwave at 150 °C for 1 h. Water (35 mL) was added to the mixture which was extracted with EtOAc thrice; the combined organic layer was dried with $MgSO_4$, concentrated and purified by silica gel chromatography to get 779 mg of ethyl 3-(3-(hydroxymethyl)phenyl)-3-(7-methoxy-1-methyl-1*H*-benzo[d][1,2,3]triazol-5-yl)propanoate **66** (55.1 %). LCMS *m/z* 370.0 $(M+H)^+$, 0.87 (ret. time).

NMR for conformational studies

NMR spectra (^1H, HSQC, ROESY) for **20**, **21**, **25** and **29** were acquired in sodium phosphate buffer (pH 7.1) on a Bruker Avance III 500 MHz spectrometer at 300 K with a 5 mm TXI cryoprobe using 2.5 mm capillary tubes with a sample volume of 160 μL (New Era). COSY spectra were also acquired for **21**, **25** and **29**. Data processing was performed using MestReNova 12 (Mestre Lab Research, Santiago de Compostela, Spain). Samples were prepared as 20 mM stocks in DMSO-d6 and diluted 20-fold with 40 mM sodium phosphate

buffer in D_2O (pH 7.1) containing a trace of TSP as internal reference to afford nominal final concentrations of 1 mM. The compounds were all soluble at this concentration as determined by quantitative NMR (QUANTAS approach[52]) using the qNMR plugin in MestReNova 12. ^1H NMR spectra with presaturation (2 s) of residual HOD were acquired with 32K (real + imaginary) data points. The real fids were zero filled to 64K and fourier transformed with an exponential line broadening of 0.4 Hz. The resulting spectra were baseline corrected and referenced to TSP (0 ppm). ROESY spectra with presaturation (2 s) of residual HOD and mixing time (250 ms) were acquired with a sweep width of 14 ppm with 2K (real + imaginary) data points in f2 and 256 (real + imaginary) increments in f1. The f2 dimension was zero-filled to afford 2048 real data points. Linear prediction was applied to the f1 dimension to afford 256 real data points that were also zero-filled to 2048. Both dimensions were fourier transformed with a 90° sine squared window function and base line corrected. %ROE measurements were taken from slices in f2 at the f1 chemical shift of interest using deconvoluted peak areas obtained directly from peak picking or from line fitting. The peak area of the hydrogen of interest was scaled to -100%.

20 3-(7-methoxy-1-methyl-1H-1,2,3-benzotriazol-5-yl)-3-{4-methyl-3-[(N-methylbenzenesulfonamido)methyl]phenyl}propanoic acid. ^1H NMR (500 MHz, 40 mM sodium phosphate pH 7.1 in D_2O) δ 7.79 – 7.73 (m, 2H), 7.72 – 7.65 (m, 1H), 7.58 (t, J = 7.8 Hz, 2H), 7.42 (d, J = 1.1 Hz, 1H), 7.28 (dd, J = 7.9, 2.0 Hz, 1H), 7.19 (d, J = 7.9 Hz, 1H), 7.11 (d, J = 1.9 Hz, 1H), 6.86 – 6.82 (m, 1H), 4.54 (t, J = 8.1 Hz, 1H), 4.37 (s, 3H), 4.13 (s, 2H), 3.92 (s, 3H), 3.02 – 2.89 (m, 2H), 2.54 (s, 3H), 2.25 (s, 3H).

21 3-{3-[(1,1-dioxo-3,4-dihydro-2H-5,1λ⁶,2-benzoxathiazepin-2-yl)methyl]-4-methylphenyl}-3-(7-methoxy-1-methyl-1H-1,2,3-benzotriazol-5-yl)propanoic acid. ^1H NMR (500 MHz, 40 mM sodium phosphate pH 7.1 in D_2O) δ 7.72 (dd, J = 7.8, 1.7 Hz, 1H), 7.65 (td, J = 7.8, 1.7 Hz, 1H), 7.43 (s, 1H), 7.32 (td, J = 7.7, 1.1 Hz, 1H), 7.32 – 7.26 (m, 2H),

7.19 (d, *J* = 7.9 Hz, 1H), 7.15 (d, *J* = 1.9 Hz, 1H), 6.85 (d, *J* = 1.2 Hz, 1H), 4.54 (t, *J* = 8.1 Hz 1H), 4.40 (s, 3H), 4.17 (t, *J* = 4.3 Hz, 2H), 4.11 (s, 2H), 3.94 (s, 3H), 3.54 (s, 2H), 3.06 – 2.88 (m, 2H), 2.22 (s, 3H).

25 (mixture of 4 stereoisomers). 3-(7-methoxy-1-methyl-1H-1,2,3-benzotriazol-5-yl)-3-{3-[(4-methyl-1,1-dioxo-3,4-dihydro-2H-5,1λ^6,2-benzoxathiazepin-2-yl)methyl]phenyl}-propanoic acid. ^{1}H NMR (500 MHz, 40 mM sodium phosphate pH 7.1 in D_2O) δ 7.79 – 7.71 (m, 1H), 7.62 – 7.49 (m, 1H), 7.43 – 7.39 (m, 1H), 7.39 – 7.35 (m, 1H), 7.34 – 7.25 (m, 2H), 7.20 – 7.15 (m, 1H), 7.15 – 7.04 (m, 2H), 6.84 – 6.78 (m, 1H), 4.58 – 4.50 (m, 1H), 4.45 – 4.38 (m, 3H), 4.34 (d, *J* = 15.1 Hz, 1H), 4.18 – 4.10 (m, 1H), 3.98 – 3.91 (m, 3H), 3.91 – 3.82 (m, 1H), 3.82 – 3.73 (m, 1H), 3.26 – 3.16 (m, 1H), 3.04 – 2.87 (m, 2H), 1.14 – 1.07 (m, 3H).

29 (3S)-3-(7-methoxy-1-methyl-1H-1,2,3-benzotriazol-5-yl)-3-(4-methyl-3-{[(4R)-4-methyl-1,1-dioxo-3,4-dihydro-2H-5,1λ^6,2-benzoxathiazepin-2-yl]methyl}phenyl)propanoic acid. ^{1}H NMR (500 MHz, 40 mM sodium phosphate pH 7.1 in D_2O) δ 7.77 (dd, *J* = 7.8, 1.7 Hz, 1H), 7.67 (td, *J* = 7.8, 1.7 Hz, 1H), 7.46 (s, 1H), 7.36 (d, *J* = 7.7 Hz, 1H), 7.36 – 7.31 (m, 1H), 7.26 (d, *J* = 8.0 Hz, 1H), 7.22 (d, *J* = 7.8 Hz, 1H), 7.04 (d, *J* = 2.0 Hz, 1H), 6.85 (s, 1H), 4.56 (t, *J* = 8.1 Hz, 1H), 4.42 (s, 3H), 4.41 (d, *J* = 14.5 Hz, 1H), 4.11 (dq, *J* = 10.4, 6.4 Hz, 1H), 3.94 (s, 3H), 3.82 (d, *J* = 14.7 Hz, 1H), 3.66 (dd, *J* = 15.5, 10.4 Hz, 1H), 3.00 (dd, *J* = 14.8, 8.6 Hz, 1H), 2.95 – 2.88 (m, 1H), 2.87 (d, *J* = 14.5 Hz, 1H), 2.24 (s, 3H), 1.00 (d, *J* = 6.4 Hz, 3H).

Expression and purification of mouse KEAP1 Kelch domain for crystallography

cDNA encoding the Kelch domain of mouse KEAP1 (Uniprot Q9Z2X8, residues 322-624) was cloned into a pET15b vector to incorporate a thrombin-cleavable N-terminal hexahistidine tag.

The protein was expressed in BL21 (DE3) cells, with 0.5 mM IPTG used for overnight induction at 18°C. Initial purification was carried out using Ni-affinity chromatography followed by removal of the hexahistidine tag by addition of bovine thombin (Sigma). Cleaved protein was incubated with Ni resin and benzamidine sepharose before size-exclusion chromatography using a HiPrep S75 26/60 column (GE Healthcare) equilibrated in 20 mM Tris-HCl pH 8.3, 20 mM DTT and 10 mM benzamidine. The protein was subsequently concentrated to approximately14 mg/mL for crystallography.

Expression and purification of human KEAP1 Kelch domain for FP assay and ITC

cDNA encoding the Kelch domain of human KEAP1 (Uniprot Q14145, residues 321-609) was cloned into the pDEST8 vector to incorporate a N-terminal hexahistidine tag, an Avi tag and a TEV protease cleavage site. Virus was generated using the Bac-to-Bac Baculovirus Expression System (Life Technologies). Protein was expressed in *Spodoptera frugiperda* (Sf9) cells by infection of 2 x 10^6 cells/mL in ExCell 420 medium (SAFC, St. Louis) using the TIPS method. Cells were harvested by centrifugation 72 h post-infection and processed for purification of recombinant protein. Cells were resuspended in a lysis buffer (50 mM Tris-HCl pH 7.5, 150 mM NaCl, 0.5 mM TCEP), and disrupted using an EmulsiFlex-C50 homogenizer (Avestin, Ottawa, Ontario, Canada) before clarification by centrifugation. The crude protein was then purified by Ni-affinity chromatography by imidazole gradient elution (0-300 mM imidazole in lysis buffer). The hexahistidine tag was removed by TEV protease cleavage (1:50 TEV to protein ratio (w/w)) during overnight dialysis against 50 mM Tris-HCl, pH 8.0, 150 mM NaCl at 4°C. The protein was finally purified by size exclusion chromatography using a 320 mL Superdex 75 column (GE Healthcare) equilibrated in 50 mM Tris-HCl pH 7.5, 150 mM NaCl, 0.5 mM TCEP, and 5% glycerol before concentration and storage at −80°C.

Crystallization, ligand soaking and X-ray data collection

Kelch protein was crystallized by vapour-diffusion using the hanging drop method from 0.3 – 0.6 $(NH_4)_2SO_4$, 0.4 – 1.4 M Li_2SO_4 and 0.1 M Na_3citrate-HCl pH 5.6. Crystals were soaked overnight in a solution containing 5 - 50 mM ligand (formulated from DMSO stocks), 100 mM Bis-Tris pH 7.0, 25% PEG 4K before plunge-freezing in liquid nitrogen. X-ray diffraction data were collected using a Rigaku-MSC Saturn 944+ CCD mounted on a Rigaku FR-E+ rotating anode generator or a DECTRIS EIGER1M detector mounted on a Rigaku FR-X rotating anode generator. Data processing, structure solution and ligand fitting was carried out using Astex's protein-ligand structure pipeline[53,54] using the apo mouse Kelch structure 1x2j as the starting model. Subsequent model rebuilding and refinement were carried out using AstexViewer[55], Coot[56] and Refmac[57]. Data collection and refinement statistics are presented in Supporting Information Table S3.

KEAP1 Kelch fluorescence polarization (FP) assay

Inhibition of the Kelch domain-NRF2 interaction was determined using a fluorescence polarization-based competition assay in black 384-well microplates. Each well contained either 2 nM 5′-TAMRA-NRF2 peptide (AFFAQLQLDEETGEFL) and 7 nM human KEAP1 Kelch domain (compounds **4**–**17**, **19, 29)** or 11 nM 5′-TAMRA-NRF2 peptide and 25 nM human KEAP1 Kelch domain (compounds **18**, **20**-**28)** in 50 mM Tris-HCl pH 8.0, 100 mM NaCl, 5 mM $MgCl_2$, 2 mM CHAPS, 1 mM DTT, 0.005% BSA, 1% DMSO. Fluorescence polarization (excitation 485 nm/emission 520 nm) was measured using a BMG Pherastar FS plate reader. IC_{50} values were determined by fitting the data to a four parameter logistic fit using Graphpad Prism 6.0 or Abase XE.

Isothermal Titration Calorimetry

ITC experiments were performed on a Microcal VP-ITC (Malvern Instruments Ltd) at 25°C in a buffer containing 50 mM HEPES-NaOH pH 7.5, 100 - 150 mM NaCl, 1 - 2 mM TCEP and 5% DMSO. In all experiments the compound was in the syringe and protein (human KEAP1 residues 321-609) was in the sample cell. Data analysis was performed using Origin 7.0 software. Heats of dilution were estimated using the final injections of each individual titration and subtracted before data analysis.

BEAS-2B NQO1 MTT Assay

BEAS-2B cells (ATCC) were plated in 384 well black clear-bottomed plates and were incubated overnight (37°C, 5% CO_2). On day two, the plates were centrifuged and 50 nL of compound or controls were added to the cells for 48 hours. On day four, the medium was removed from the plate and crude cell lysates were made by using 0.667X (Cell Signaling Technology, Boston MA) lysis buffer with Complete, Mini, EDTA-free Protease Inhibitor (Roche Applied Sciences, Germany). After lysis, the plates were incubated for 20 minutes at room temperature and the MTT cocktail was prepared for measurement of NQO1 activity[58]. The samples were analyzed on an Envision plate reader (Perkin Elmer), reading absorbance at 570 nm for five individual readings with 10 minute intervals. Product formation was measured kinetically and the pEC_{50} of NQO1 specific activity induction was calculated by plotting the change in absorbance (ΔOD/min) *versus* log [compound] followed by 4-parameter fitting with ActivityBase (Abase).

SUPPORTING INFORMATION

The following Figures and Tables are provided as Supporting Information: **Table S1** %ROEs for proton 15-H for compounds **21**, **25** and **29**; **Figure S1** Slices through ROESY spectrum for **29** for protons 19-H′, 19-H″ and 3-H_3; **Figure S2** ^{1}H, COSY, HSQC and ROESY spectra for compounds **20**, **21**, **25** and **29**; **Table S2** ^{1}H and ^{13}C chemical shift data for compounds **20**, **21**, **25** and **29**; **Table S3** X-ray data collection and refinement statistics; Description of conformational analysis for chloro-phenyl versus tolyl model systems. **Molecular Formula Strings** and associated FP and BEAS-2B assay data.

PDB ID CODES

Coordinates and structure factors for the KEAP1-ligand complexes described in this paper have been deposited with PDB with accession codes: 6qmc (KEAP1-**5**), 6qmd (KEAP1-(*R*)-**7**), 6qme (KEAP1-**12**), 6qmj (KEAP1-**20**), 6qmk (KEAP1-**21**). Authors will release the atomic coordinates and experimental data upon article publication.

CORRESPONDING AUTHOR INFORMATION

Dr Thomas G. Davies

Email: tom.davies@astx.com

Dr Jeffrey K. Kerns

Email: Jeffrey.K.Kerns@gsk.com

ACKNOWLEDGEMENTS

The authors thank Philip Day for the cloning of mouse Kelch, Kirsten Smith for protein expression/purification, Anne Cleasby for protein purification, structure refinement and PDB deposition, Finn Holding for mass spectrometry, Ming Jiang, Michael Fisher and John Yonchuk for FP and BEAS-2B bioassay screening and Thomas Sweitzer for helpful discussions.

ABBREVIATIONS

BTB, Broad-complex, Tramtrack and Bric-a-Brac; Cul3, Cullin 3; FP, fluorescence polarization; ITC, Isothermal Scanning Calorimetry; IVR, Intervening Region; KEAP1, Kelch-like ECH-associated protein 1; MTT, 3-(4,5-dimethylthiazol-2-yl)-2,5-diphenyltetrazolium bromide; NQO1, NAD(P)H:quinone acceptor oxidoreductase 1; NRF2, Nuclear factor erythroid 2–related factor 2; PPI, protein-ptotein interaction; Rbx1, RING-box protein 1; ROESY, Rotating frame nuclear Overhauser enhancement spectroscopy.

REFERENCES

(1) Itoh, K.; Chiba, T.; Takahashi, S.; Ishii, T.; Igarashi, K.; Katoh, Y.; Oyake, T.; Hayashi, N.; Satoh, K.; Hatayama, I.; Yamamoto, M.; Nabeshima, Y. An Nrf2/small Maf heterodimer mediates the induction of phase II detoxifying enzyme genes through antioxidant response elements. *Biochem.Biophys.Res.Commun.* **1997,** *236*, 313-322.

(2) Wakabayashi, N.; Dinkova-Kostova, A. T.; Holtzclaw, W. D.; Kang, M. I.; Kobayashi, A.; Yamamoto, M.; Kensler, T. W.; Talalay, P. Protection against electrophile and oxidant stress by induction of the phase 2 response: fate of cysteines of the Keap1 sensor modified by inducers. *Proc.Natl.Acad.Sci.U.S.A* **2004,** *101*, 2040-2045.

(3) Zhang, M.; An, C.; Gao, Y.; Leak, R. K.; Chen, J.; Zhang, F. Emerging roles of Nrf2 and phase II antioxidant enzymes in neuroprotection. *Prog.Neurobiol.* **2013,** *100*, 30-47.

(4) Zhang, D. D.; Lo, S. C.; Cross, J. V.; Templeton, D. J.; Hannink, M. Keap1 is a redox-regulated substrate adaptor protein for a Cul3-dependent ubiquitin ligase complex. *Mol.Cell Biol.* **2004,** *24*, 10941-10953.

(5) Cullinan, S. B.; Gordan, J. D.; Jin, J.; Harper, J. W.; Diehl, J. A. The Keap1-BTB protein is an adaptor that bridges Nrf2 to a Cul3-based E3 ligase: oxidative stress sensing by a Cul3-Keap1 ligase. *Mol.Cell Biol.* **2004,** *24*, 8477-8486.

(6) Canning, P.; Cooper, C. D.; Krojer, T.; Murray, J. W.; Pike, A. C.; Chaikuad, A.; Keates, T.; Thangaratnarajah, C.; Hojzan, V.; Marsden, B. D.; Gileadi, O.; Knapp, S.; von, D. F.; Bullock, A. N. Structural basis for Cul3 protein assembly with the BTB-Kelch family of E3 ubiquitin ligases. *J.Biol.Chem.* **2013,** *288*, 7803-7814.

(7) Cleasby, A.; Yon, J.; Day, P. J.; Richardson, C.; Tickle, I. J.; Williams, P. A.; Callahan, J. F.; Carr, R.; Concha, N.; Kerns, J. K.; Qi, H.; Sweitzer, T.; Ward, P.; Davies, T. G. Structure

of the BTB domain of Keap1 and its interaction with the triterpenoid antagonist CDDO. *PLoS One* **2014,** *9*, e98896.

(8) Li, X.; Zhang, D.; Hannink, M.; Beamer, L. J. Crystal structure of the Kelch domain of human Keap1. *J.Biol.Chem.* **2004,** *279*, 54750-54758.

(9) Dinkova-Kostova, A. T.; Holtzclaw, W. D.; Cole, R. N.; Itoh, K.; Wakabayashi, N.; Katoh, Y.; Yamamoto, M.; Talalay, P. Direct evidence that sulfhydryl groups of Keap1 are the sensors regulating induction of phase 2 enzymes that protect against carcinogens and oxidants. *Proc.Natl.Acad.Sci.U.S.A* **2002,** *99*, 11908-11913.

(10) Zhang, D. D.; Hannink, M. Distinct cysteine residues in Keap1 are required for Keap1-dependent ubiquitination of Nrf2 and for stabilization of Nrf2 by chemopreventive agents and oxidative stress. *Mol.Cell Biol.* **2003,** *23*, 8137-8151.

(11) Rachakonda, G.; Xiong, Y.; Sekhar, K. R.; Stamer, S. L.; Liebler, D. C.; Freeman, M. L. Covalent modification at Cys151 dissociates the electrophile sensor Keap1 from the ubiquitin ligase CUL3. *Chem.Res.Toxicol.* **2008,** *21*, 705-710.

(12) Eggler, A. L.; Small, E.; Hannink, M.; Mesecar, A. D. Cul3-mediated Nrf2 ubiquitination and antioxidant response element (ARE) activation are dependent on the partial molar volume at position 151 of Keap1. *Biochem.J.* **2009,** *422*, 171-180.

(13) Kensler, T. W.; Wakabayashi, N.; Biswal, S. Cell survival responses to environmental stresses via the Keap1-Nrf2-ARE pathway. *Annu.Rev.Pharmacol.Toxicol.* **2007,** *47*, 89-116.

(14) Wasserman, W. W.; Fahl, W. E. Functional antioxidant responsive elements. *Proc.Natl.Acad.Sci.U.S.A* **1997,** *94*, 5361-5366.

(15) Cho, H. Y.; Kleeberger, S. R. Nrf2 protects against airway disorders. *Toxicol.Appl.Pharmacol.* **2010,** *244*, 43-56.

(16) Boutten, A.; Goven, D.; Artaud-Macari, E.; Boczkowski, J.; Bonay, M. NRF2 targeting: a promising therapeutic strategy in chronic obstructive pulmonary disease. *Trends Mol Med* **2011,** *17*, 363-71.

(17) Calkins, M. J.; Johnson, D. A.; Townsend, J. A.; Vargas, M. R.; Dowell, J. A.; Williamson, T. P.; Kraft, A. D.; Lee, J. M.; Li, J.; Johnson, J. A. The Nrf2/ARE pathway as a potential therapeutic target in neurodegenerative disease. *Antioxid.Redox.Signal.* **2009,** *11*, 497-508.

(18) Li, J.; Ichikawa, T.; Janicki, J. S.; Cui, T. Targeting the Nrf2 pathway against cardiovascular disease. *Expert.Opin.Ther.Targets.* **2009,** *13*, 785-794.

(19) Pergola, P. E.; Raskin, P.; Toto, R. D.; Meyer, C. J.; Huff, J. W.; Grossman, E. B.; Krauth, M.; Ruiz, S.; Audhya, P.; Christ-Schmidt, H.; Wittes, J.; Warnock, D. G. Bardoxolone methyl and kidney function in CKD with type 2 diabetes. *N.Engl.J.Med.* **2011,** *365*, 327-336.

(20) Cuadrado, A.; Rojo, A. I.; Wells, G.; Hayes, J. D.; Cousin, S. P.; Rumsey, W. L.; Attucks, O. C.; Franklin, S.; Levonen, A. L.; Kensler, T. W.; Dinkova-Kostova, A. T. Therapeutic targeting of the NRF2 and KEAP1 partnership in chronic diseases. *Nat Rev Drug Discov* **2019,** *18*, 295-317.

(21) Bewley, M. A.; Budd, R. C.; Ryan, E.; Cole, J.; Collini, P.; Marshall, J.; Kolsum, U.; Beech, G.; Emes, R. D.; Tcherniaeva, I.; Berbers, G. A. M.; Walmsley, S. R.; Donaldson, G.; Wedzicha, J. A.; Kilty, I.; Rumsey, W.; Sanchez, Y.; Brightling, C. E.; Donnelly, L. E.; Barnes, P. J.; Singh, D.; Whyte, M. K. B.; Dockrell, D. H.; Copdmap. Opsonic Phagocytosis in Chronic Obstructive Pulmonary Disease is enhanced by Nrf2 agonists. *Am J Respir Crit Care Med* **2018,** *198*, 739-750.

(22) Linker, R. A.; Lee, D. H.; Ryan, S.; van Dam, A. M.; Conrad, R.; Bista, P.; Zeng, W.; Hronowsky, X.; Buko, A.; Chollate, S.; Ellrichmann, G.; Bruck, W.; Dawson, K.; Goelz, S.; Wiese, S.; Scannevin, R. H.; Lukashev, M.; Gold, R. Fumaric acid esters exert neuroprotective

effects in neuroinflammation via activation of the Nrf2 antioxidant pathway. *Brain* **2011,** *134*, 678-692.

(23) de Zeeuw, D.; Akizawa, T.; Audhya, P.; Bakris, G. L.; Chin, M.; Christ-Schmidt, H.; Goldsberry, A.; Houser, M.; Krauth, M.; Lambers Heerspink, H. J.; McMurray, J. J.; Meyer, C. J.; Parving, H. H.; Remuzzi, G.; Toto, R. D.; Vaziri, N. D.; Wanner, C.; Wittes, J.; Wrolstad, D.; Chertow, G. M.; Investigators, B. T. Bardoxolone methyl in type 2 diabetes and stage 4 chronic kidney disease. *N Engl J Med* **2013,** *369*, 2492-2503.

(24) Sussan, T. E.; Rangasamy, T.; Blake, D. J.; Malhotra, D.; El-Haddad, H.; Bedja, D.; Yates, M. S.; Kombairaju, P.; Yamamoto, M.; Liby, K. T.; Sporn, M. B.; Gabrielson, K. L.; Champion, H. C.; Tuder, R. M.; Kensler, T. W.; Biswal, S. Targeting Nrf2 with the triterpenoid CDDO-imidazolide attenuates cigarette smoke-induced emphysema and cardiac dysfunction in mice. *Proc.Natl.Acad.Sci.U.S.A* **2009,** *106*, 250-255.

(25) Wilson, A. J.; Kerns, J. K.; Callahan, J. F.; Moody, C. J. Keap calm - and carry on covalently. *J.Med.Chem.* **2013,** *56*, 7463-7476.

(26) Hancock, R.; Bertrand, H. C.; Tsujita, T.; Naz, S.; El-Bakry, A.; Laoruchupong, J.; Hayes, J. D.; Wells, G. Peptide inhibitors of the Keap1-Nrf2 protein-protein interaction. *Free Radic.Biol.Med.* **2012,** *52*, 444-451.

(27) Abed, D. A.; Goldstein, M.; Albanyan, H.; Jin, H.; Hu, L. Discovery of direct inhibitors of Keap1-Nrf2 protein-protein interaction as potential therapeutic and preventive agents. *Acta Pharm Sin B* **2015,** *5*, 285-299.

(28) Zhuang, C.; Miao, Z.; Sheng, C.; Zhang, W. Updated Research and Applications of Small Molecule Inhibitors of Keap1-Nrf2 Protein-Protein Interaction: a Review. *Curr.Med.Chem.* **2014,** *21*, 1861-1870.

(29) Pallesen, J. S.; Tran, K. T.; Bach, A. Non-covalent Small-Molecule Kelch-like ECH-Associated Protein 1-Nuclear Factor Erythroid 2-Related Factor 2 (Keap1-Nrf2) inhibitors and

their potential for targeting Central Nervous System diseases. *J Med Chem* **2018,** *61*, 8088-8103.

(30) Padmanabhan, B.; Tong, K. I.; Ohta, T.; Nakamura, Y.; Scharlock, M.; Ohtsuji, M.; Kang, M. I.; Kobayashi, A.; Yokoyama, S.; Yamamoto, M. Structural basis for defects of Keap1 activity provoked by its point mutations in lung cancer. *Mol.Cell* **2006,** *21*, 689-700.

(31) Lo, S. C.; Li, X.; Henzl, M. T.; Beamer, L. J.; Hannink, M. Structure of the Keap1:Nrf2 interface provides mechanistic insight into Nrf2 signaling. *EMBO J.* **2006,** *25*, 3605-3617.

(32) Tong, K. I.; Katoh, Y.; Kusunoki, H.; Itoh, K.; Tanaka, T.; Yamamoto, M. Keap1 recruits Neh2 through binding to ETGE and DLG motifs: characterization of the two-site molecular recognition model. *Mol.Cell Biol.* **2006,** *26*, 2887-2900.

(33) Tong, K. I.; Kobayashi, A.; Katsuoka, F.; Yamamoto, M. Two-site substrate recognition model for the Keap1-Nrf2 system: a hinge and latch mechanism. *Biol.Chem.* **2006,** *387*, 1311-1320.

(34) Tong, K. I.; Padmanabhan, B.; Kobayashi, A.; Shang, C.; Hirotsu, Y.; Yokoyama, S.; Yamamoto, M. Different electrostatic potentials define ETGE and DLG motifs as hinge and latch in oxidative stress response. *Mol.Cell Biol.* **2007,** *27*, 7511-7521.

(35) Jiang, Z. Y.; Lu, M. C.; You, Q. D. Discovery and Development of Kelch-like ECH-Associated Protein 1. Nuclear Factor Erythroid 2-Related Factor 2 (KEAP1:NRF2) Protein-Protein Interaction inhibitors: achievements, challenges, and future directions. *J Med Chem* **2016,** *59*, 10837-10858.

(36) Davies, T. G.; Wixted, W. E.; Coyle, J. E.; Griffiths-Jones, C.; Hearn, K.; McMenamin, R.; Norton, D.; Rich, S. J.; Richardson, C.; Saxty, G.; Willems, H. M.; Woolford, A. J.; Cottom, J. E.; Kou, J. P.; Yonchuk, J. G.; Feldser, H. G.; Sanchez, Y.; Foley, J. P.; Bolognese, B. J.; Logan, G.; Podolin, P. L.; Yan, H.; Callahan, J. F.; Heightman, T. D.; Kerns, J. K. Monoacidic inhibitors of the Kelch-like ECH-Associated Protein 1: Nuclear Factor Erythroid 2-Related

Factor 2 (KEAP1:NRF2) Protein-Protein interaction with high cell potency identified by Fragment-Based Discovery. *J Med Chem* **2016,** *59*, 3991-4006.

(37) Tamanini, E.; Buck, I. M.; Chessari, G.; Chiarparin, E.; Day, J. E. H.; Frederickson, M.; Griffiths-Jones, C. M.; Hearn, K.; Heightman, T. D.; Iqbal, A.; Johnson, C. N.; Lewis, E. J.; Martins, V.; Peakman, T.; Reader, M.; Rich, S. J.; Ward, G. A.; Williams, P. A.; Wilsher, N. E. Discovery of a potent nonpeptidomimetic, small-molecule antagonist of Cellular Inhibitor of Apoptosis Protein 1 (cIAP1) and X-Linked Inhibitor of Apoptosis Protein (XIAP). *Journal of Medicinal Chemistry* **2017,** *60*, 4611-4625.

(38) Veber, D. F.; Johnson, S. R.; Cheng, H. Y.; Smith, B. R.; Ward, K. W.; Kopple, K. D. Molecular properties that influence the oral bioavailability of drug candidates. *J.Med.Chem.* **2002,** *45*, 2615-2623.

(39) Chen, C. Y.; Andreani, T.; Li, H. A divergent and selective synthesis of isomeric benzoxazoles from a single N-Cl imine. *Org Lett* **2011,** *13*, 6300-3.

(40) Sakai, M.; Hayashi, H.; Miyaura, N. Rhodium-catalyzed conjugate addition of aryl- or 1-Alkenylboronic acids to enones. *Organometallics* **1997,** *16*, 4229-4231.

(41) Brewerton, S. C. The use of protein-ligand interaction fingerprints in docking. *Curr Opin Drug Discov Devel* **2008,** *11*, 356-364.

(42) Marcou, G.; Rognan, D. Optimizing fragment and scaffold docking by use of molecular interaction fingerprints. *J.Chem.Inf.Model.* **2007,** *47*, 195-207.

(43) Deng, Z.; Chuaqui, C.; Singh, J. Structural interaction fingerprint (SIFt): a novel method for analyzing three-dimensional protein-ligand binding interactions. *J Med Chem* **2004,** *47*, 337-344.

(44) Rognan, D. Fragment-based approaches and computer-aided drug discovery. *Top Curr Chem* **2012,** *317*, 201-222.

(45) Rathi, P. C.; Ludlow, R. F.; Hall, R. J.; Murray, C. W.; Mortenson, P. N.; Verdonk, M. L. Predicting "hot" and "warm" spots for fragment binding. *J Med Chem* **2017,** *60*, 4036-4046.

(46) Yang, L.; Adam, C.; Nichol, G. S.; Cockroft, S. L. How much do van der Waals dispersion forces contribute to molecular recognition in solution? *Nature Chemistry* **2013,** *5*, 1006-1010.

(47) Nayak, S. K.; Sathishkumar, R.; Row, T. N. G. Directing role of functional groups in selective generation of C-H...pi interactions: In situ cryo-crystallographic studies on benzyl derivatives. *CrystEngComm* **2010,** *12*, 3112-3118.

(48) Di Fabio, R.; Pellacani, A.; Faedo, S.; Roth, A.; Piccoli, L.; Gerrard, P.; Porter, R. A.; Johnson, C. N.; Thewlis, K.; Donati, D.; Stasi, L.; Spada, S.; Stemp, G.; Nash, D.; Branch, C.; Kindon, L.; Massagrande, M.; Poffe, A.; Braggio, S.; Chiarparin, E.; Marchioro, C.; Ratti, E.; Corsi, M. Discovery process and pharmacological characterization of a novel dual orexin 1 and orexin 2 receptor antagonist useful for treatment of sleep disorders. *Bioorganic & Medicinal Chemistry Letters* **2011,** *21*, 5562-5567.

(49) Yin, J.; Babaoglu, K.; Brautigam, C. A.; Clark, L.; Shao, Z.; Scheuermann, T. H.; Harrell, C. M.; Gotter, A. L.; Roecker, A. J.; Winrow, C. J.; Renger, J. J.; Coleman, P. J.; Rosenbaum, D. M. Structure and ligand-binding mechanism of the human OX1 and OX2 orexin receptors. *Nature Structural &Amp; Molecular Biology* **2016,** *23*, 293-299.

(50) Do, T. N.; Choy, W. Y.; Karttunen, M. Accelerating the Conformational Sampling of Intrinsically Disordered Proteins. *J Chem Theory Comput* **2014,** *10*, 5081-5094.

(51) Do, T. N.; Choy, W. Y.; Karttunen, M. Binding of disordered peptides to Kelch: insights from enhanced sampling simulations. *J Chem Theory Comput* **2016,** *12*, 395-404.

(52) Farrant, R. D.; Hollerton, J. C.; Lynn, S. M.; Provera, S.; Sidebottom, P. J.; Upton, R. J. NMR quantification using an artificial signal. *Magn Reson Chem* **2010,** *48*, 753-762.

(53) Mooij, W. T.; Hartshorn, M. J.; Tickle, I. J.; Sharff, A. J.; Verdonk, M. L.; Jhoti, H. Automated protein-ligand crystallography for structure-based drug design. *ChemMedChem.* **2006,** *1*, 827-838.

(54) Davies, T. G.; Tickle, I. J. Fragment screening using X-ray crystallography. *Top.Curr.Chem.* **2012,** *317*, 33-59.

(55) Hartshorn, M. J. AstexViewer: a visualisation aid for structure-based drug design. *J.Comput.Aided Mol.Des* **2002,** *16*, 871-881.

(56) Emsley, P.; Cowtan, K. Coot: model-building tools for molecular graphics. *Acta Crystallogr.D.Biol.Crystallogr.* **2004,** *60*, 2126-2132.

(57) Murshudov, G. N.; Vagin, A. A.; Dodson, E. J. Refinement of macromolecular structures by the maximum-likelihood method. *Acta Crystallogr D Biol Crystallogr* **1997,** *53*, 240-255.

(58) Prochaska, H. J.; Santamaria, A. B. Direct measurement of NAD(P)H:quinone reductase from cells cultured in microtiter wells: a screening assay for anticarcinogenic enzyme inducers. *Anal Biochem* **1988,** *169*, 328-236.

FIGURE LEGENDS

Figure 1 The KEAP1 Kelch domain and NRF2 PPI. (a) Cartoon representation of the Kelch domain with a 9-mer NRF2-derived peptide bound (orange). Figures presented in this paper showing NRF2-bound KEAP1 were generated from the structure by Padmanabhan *et al*[30] (PDB code 1x2r). Chemical structure of the KEAP1-NRF2 PPI inhibitor KI-696[36]. (b) Chemical structures of the three fragment hits described, and detail of the NRF2 binding site showing experimentally observed positions of fragment binding in the context of the KEAP1-bound NRF2 peptide (orange). The protein surface is coloured to highlight the three hot-spots identified from the fragment screen (red="Planar Acceptor"; green="Acid"; purple ="Sulfonamide"). (c) Design strategy to exploit growth vectors from the chloro-phenyl propionic acid hit towards the Planar Acceptor and Sulfonamide hot-spots. The KEAP1-fragment co-complex structures used to generate (b) and (c) have been deposited previously with PDB codes 5fnq (**1**), 5fzj (**2**), 5fzn (**3**)[36].

Figure 2 Fragment growth from chlorophenyl propionic acid **1** to compound **15** guided by KEAP1 co-complex structures. The NRF2 binding site of the KEAP1 Kelch domain is shown as a grey transparent surface with key residues highlighted. Hydrogen bonding and electrostatic interactions described in the text are shown as dashed lines. Co-complex structures are presented as follows (PDB code in parentheses): (a) KEAP-**1** (5fnq[36]) (b) KEAP-**5** (6qmc); (c) KEAP-**7** (5fnr[36]); (d) KEAP-**12** (6qme); (e) KEAP-**14** (5fns[36]); (f) KEAP-**15** (5fnt[36]).

Figure 3 Structure of the KEAP1-(*R*)-**7** co-complex (PDB code 6qmd). Two binding events within the NRF2-site were observed for (*R*)-**7** when soaked at 50 mM ligand concentration.

The canonical binding mode is shown with carbon atoms coloured green, and the additional, weaker binding mode is shown with carbon atoms coloured white. The protein surface is coloured according to lipophilicity as calculated within AstexViewer[55] (from red/orange for the most lipophilic areas to green/blue for polar areas). The final $2mF_o$-DF_c electron density (contoured at 1σ) for the additional binding mode is shown as a green mesh.

Figure 4 Addressing the high energy conformation for KEAP1-bound **15**. (a) Structure of KEAP1-**15** co-complex (PDB code 5fnt[36]). The putative unfavourable polar contact is shown as a red dashed line. (b) Electrostatic surfaces for chloro-phenyl and tolyl, calculated using density function theory with the B3LYP functional and the 6-31G* basis set. Surfaces are coloured from red (most negative potential) to blue (most positive potential). (c) Model system for 3-dimensional conformational energy search (X = Cl or Me). Dihedrals explored during the conformational search are highlighted with red arrows.

Figure 5 Optimization of compound **20** to **29**. (a) Structure of KEAP1-**20** (PDB code 6qmj). (b) Structure of KEAP1-**20** (green carbons) overlaid with bound structure of **21** (PDB code 6qmk; cyan carbons). (c) Van der Waals surface for the KEAP1-bound **21** showing the void (marked *) between benzotriazole and oxathiazepine moieties. (d) Structure of KEAP1-**29** (PDB code 5fnu[36]; yellow carbons) overlaid with bound structure of **21** (cyan carbons). (e) Van der Waals surface for KEAP1-bound **29** showing partial filling of void described in (c) by the pendant methyl. (f) Overlay of KEAP1-**29** (yellow carbons) with second copy of KEAP1-bound (*R*)-**7** (PDB code 6qmd; white carbons). The chloro-phenyl of (*R*)-**7** occupies the same region of the NRF2 binding site as the pendant methyl in **29**.

Figure 6 1D NMR conformational signatures of compound **29** (KI-696) and analogues. (a) Chemical structure of **29** and numbering system used for the NMR discussion, highlighting key hydrogens diagnostic of conformational restriction. (b) Partial ^{1}H NMR spectra in 40 mM phosphate buffer pH 7.4 for **20**, **21**, **25** and **29**: changes in chemical shifts for hydrogens of the seven-membered ring (**21**, **25**, **29**) and methylene linker are highlighted according to scheme (a). (c) Selected ROEs for free **29** shown in the context of the Kelch-bound conformation (taken from PDB code 5fnu[36]). ROEs consistent with the bound conformation are indicated as solid curved arrows. Dotted curved arrows indicate observed ROEs consistent with a "collapsed" conformation, although potentially requiring minor torsional adjustments relative to the bound state (eg around C19-C29 and/or C28-C36 bonds). The putative hydrophobic collapse between benzotriazole and the oxathiazepine is highlighted with a black arrow.

TABLE OF CONTENTS GRAPHIC

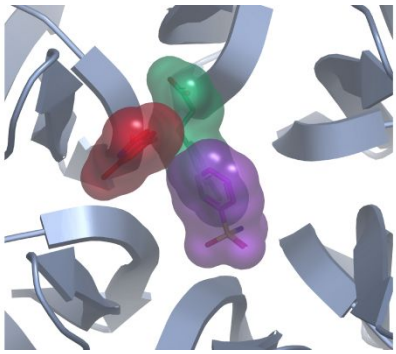

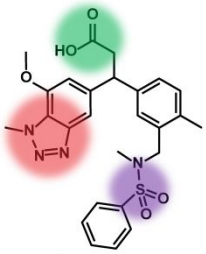

20 BEAS-2B EC_{50} = 850 nM
Hot-spot optimization

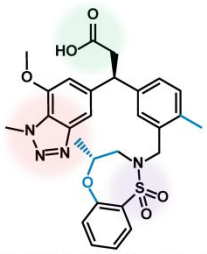

29 BEAS-2B EC_{50} = 12 nM
Ligand preorganization